Electrochemical Post-Processing of Zn-Ni Deposition on Steel Substrate for Reliable Composition

Capstone Final Report

MSE 4952 - Materials Design and Capstone II

The University of Virginia

In Collaboration with Rolls-Royce Corporation and Luna Labs USA LLC

By Thomas Domer, Emma Laubengayer, Morgan Small, Leah Smith, and Alexandra Uy

Date: May 1, 2024

Contact Information

Collaborators

Dr. Robert Golden, of Rolls-Royce Corporation (robert.golden@rolls-royce.com)

Brad Wiley, of Rolls-Royce Corporation (brad.wiley@rolls-royce.com)

Dr. Rebecca Marshall, of Luna Labs USA LLC (rebecca.marshall@lunalabs.us)

Victoria Avance, of Luna Labs USA LLC (vic.avance@lunalabs.us)

UVA Mentorship

Dr. James Fitz-Gerald, Capstone Advisor (jmf8h@virginia.edu)

Dr. Robert Kelly, Subject Matter Expert, (rgk6y@virginia.edu)

Ph.D. Candidate Victor Kontopanos, (cnm5nn@virginia.edu)

Authors

Thomas Domer (tjd4ddv@virginia.edu)

Emma Laubengayer (ell5mus@virginia.edu)

Morgan Small (mks4kw@virginia.edu)

Leah Smith (las4dgs@virginia.edu)

Alexandra Uy (awu4mw@virginia.edu

Table of Contents

Table of Figures

Executive Summary

Mission Statement and Objective

The aim of this project was intended to reduce stress corrosion cracking (SCC) behavior in a zinc nickel (Zn-Ni) electroplated deposit on steel panel substrates under high stress field conditions by optimizing the composition of the Zn-Ni coating within a range of 12-15 wt% Ni. The method selected for creating a Zn-Ni coating immune to stress corrosion cracking was to tailor the Ni content through selective dissolution of Zn. The objective was to consistently raise the open circuit potential (OCP) of Zn-Ni coated steel to between –0.7 and –0.3 V vs SCE.

Instrumentation and Project Materials

NAVAIR Patuxent River assisted the team by providing the solution components for the DIPSOL IZ-C17+ solution which was necessary for the experimental portion of the capstone project. Two steel plates were provided by Rolls-Royce Corporation (RR) were sectioned into 0.75” squares, providing 60 usable samples for experimentation. These were then divided into two batches- designated as batch 3 and batch 4- based on the plate from which they were cut. Selected samples underwent scanning electron microscopy (SEM) and thus, were first mounted for plan view microscopy in fast-cure epoxy before sectioning with a low-speed saw down the middle of their experimentation regions. For further characterization, samples were mounted in a cross-section orientation, ground and polished down, and sputter coated with Au-Pd prior to SEM and energy dispersive edroscopy (EDS) characterization. Sputter coating was performed with the Cressington and SEM/EDS characterization was conducted with the FEI Quanta 650 and the attached Oxford EDS detector all housed in the University of Virginia (UVA) Nanoscale Materials Characterization Facility (NMCF). All X-ray diffraction (XRD) characterization was performed using Empyrean Multipurpose X-Ray Diffractometer produced by Malvern Panalytical, which is also housed in the UVA NMCF. The XRD data was then processed using the software HighScore, produced by Malvern Panalytical.

Results

Multiple attempts were made to identify a replicable selective dissolution process to reach the potential range of interest. Once the replicable technique had been established, it was necessary to see if it was viable on a batch of samples which underwent different coating deposition processing. However, SEM characterization found that all successful samples from

both batches had all of the coating stripped away, baring the substrate material, regardless of any difference in coating thickness. The change in OCP was not from the selective dissolution of Zn from the Zn-Ni coating. It seems more likely that the exposure of the more noble substrate material led to the OCP being within the potential region of interest.

For the conditions used, it appears that the coating was completely dissolved from the substrate. Suggestions to improve the experiment include using thicker coatings, using coatings with higher initial Ni contents to start, or accepting the use of lower current densities albeit leading to longer treatment times.

Project Timeline

Table 1. GANTT Chart Indicating Project Timeline

	Dates:	1-Nov	15-Nov	1-Dec	15-Dec	Winter Break	15-Jan	1-Feb	15-Feb	1-Mar	15-Mar	1-Apr	15-Apr	1-May	15-May
Benchmarks:															
Literature review on general Zn-Ni															
Receiving samples															
Preliminary sectioning															
Preliminary characterization (SEM/EDS)															
Literature review on trivalent chromium passivate layers															
Design passivate layer removal															
Build passivate layer removal system															
Informed removal of passivate layer															
Informed sectioning (with sample prep, ex. Mounting)															
Literature review on solutionizing out solid constituents															
Design bath set up															
Deplete DIPSOL of Zn															
Build bath set up															
Experimentation- removing Zn preferentially from Zn-Ni															
XRD characterization															
XRD analysis in High Score and GSAS-II/Rietvelt															
SEM/EDS charaterization															
SEM analysis in ImageJ, EDS analysis in Aztec															
Micro X-ray CT characterization															
Modify Python algorithm for our experiment															
CT analysis using Python algorithm															
Compile final documentation															
Compile final presentation															
Rehearse presentation															
Finished with capstone!!!															

Table 1 contains the GANTT chart that was used to track and document important benchmarks to guide the project towards completion.

These benchmarks were pursued within reason, some proved superfluous or outside of this project's scope. Originally, there had been the intention to remove the trivalent chromium passivate layer that coats some of the as-received plates, but upon deeper review, it was understood that during the selective dissolution technique, this additional layer would be pulled off as well. Thus, it was found that pursuing an additional removal process was not needed. The Center for Electrochemical Science and Engineering Laboratory provided electrochemical plating cells. It was also identified that the depletion of Zn from the DIPSOL IZ-C17+ solution reflected operating conditions, and thus this was not pursued. The last difference in benchmarks from the original plan is that the micro-X-ray computed tomography (CT) characterization was not pursued due to the availability of industry partners.

Broadly, the original plan was similar to the execution, but in contrast with the original outline, the windows of experimentation and characterization were extended, while documentation and presentation were scheduled sooner into the semester than the original plan.

Cost Data and Constraints

Cost Data

In Table 2, all cost data associated with the project is displayed.

Table 2: Cost Summary Table

Task and Materials	Cost per hour ($/hr)	Estimated time (hr)	Total cost ($)
Electrochemical solutions (DIPSOL and NaCl)	*	-	0
Steel panels	*	-	0
Stir plates and electrochemical cells	*	-	0
Sectioning	50	2	100
Cross-section/mounting	*	6	0
Grinding/polishing	-	3	70
Sputtering	17 (per job)	5 jobs	85
XRD	39	2	78
SEM/EDS	39/50 (after/before 5pm)	17	850
Total			**1183**

Any costs denoted with an asterisk (*) were effectively free.

Metric for Completion

The metric for success in this study was originally to reliably and repeatedly be able to achieve a targeted Zn-Ni ratio.

The metric for success in this study was to reliably and repeatedly be able to achieve immunity to stress corrosion cracking (SCC) given a specific current density for the electrochemical cell and a specific duration for exposure in the cell. The metric for completion was to either achieve the metric for success or to identify that this is not achievable given the constraints, including time, available materials, and techniques. To address this, the target post-experimentation OCP was between –0.7 and –0.3 V vs SCE, where the Zn-Ni coatings are functionally immune to SCC (Harris et al., 2023).

Constraints

The experimental and characterization procedures were constrained by time, sample composition, and the selective dissolution technique. The electroplated panels used in this experimentation were compromised of the same composition and underwent the same processing by prior work by RR. When this is implemented for use, this technique will optimize Zn-Ni coated Pyrowear, which is a specialty steel alloy, whereas the samples received for this experimentation were a carbon steel substrate instead. For the selective dissolution, the DIPSOL IZ-C17+ solution was used to maximize convenience when integrating this research into the current industry procedure. Current densities were tested so that the selective dissolution could

take place between 20-60 minutes to prevent prohibitively long duration compared to the initial Zn-Ni deposition.

Time

The optimization of the selective dissolution process had a delivery deadline of mid-May 2024, given that this project was assigned to begin in August 2023. The overall time allocated to this project was 9 months. A GANTT Chart detailing the progress on the capstone project is seen in Table 1 below. The period allotted for experimentation and iteration of the optimized selective dissolution technique was limited to the 15th of January to the beginning of April 2024. This is because the DIPSOL IZ-C17+ electrodeposition solution was retrieved in mid-January 2024. Following experimentation, the beginning of April 2024 marked the period of which documentation was to be finalized. Thus, the optimization of the technique is limited to a 3-month period.

Sample Composition and Sectioning Constraints

The steel plates received from RR had a trivalent chromate coating layer on top of the Zn-Ni coating because that is currently required of their final products. Thus, to target the Zn-Ni coating beneath the trivalent chromate layer, removal of this layer was considered. Though, this would not be a concern if the selective dissolution could be performed prior to chromate application and after Zn-Ni deposition. One concern with this was that the trivalent chromate coating might interfere with the selective dissolution. However, it was reasonable to assume it was thin enough to dissolve along with the Zn-Ni, and the experimental results suggest that the impact of the chromate was negligible for this project.

Post-experimentation, samples were sectioned for requisite cross-section characterization. These samples were mounted in long-cure epoxy before sectioning because the steel plates were thin, and this caused concern for fracture. After this, the samples were then mounted in a cross-section view to examine the coatings from the side. These samples were ground, polished, and sputter coated with ~14nm of Au-Pd to help mitigate charge buildup under SEM. In one batch of samples, contamination was introduced in the interval between sample preparation and characterization. It is unclear what caused this contamination. It appeared as particulate on the surface of several cross-sectional samples, which significantly obscured the surface. The particulate was not able to be fully removed, but micrographs were taken in less obstructed surfaces.

Selective Dissolution Optimization Constraints

RR outsources their electrochemical deposition to TechMetals, a company with the requisite plating capabilities. The plating bath utilized by TechMetals to deposit the Zn-Ni electrodeposited coating is comprised of the DIPSOL IZ-C17+ solution. For the selective dissolution technique to be viable in industry, the technique must work within the current plating solution. The DIPSOL IZ-C17+ solution components were obtained directly from NAVAIR Patuxent River through an industry partnership. Each component had a volume of around 1 gallon. Relative to the needs of this project, this supply exceeded the experimental need.

Methodology

Electrochemical Methods

Experimentation comprised of a range of electrochemical techniques. Specifically, electrochemistry is fundamental to the electrodeposition process. The primary electrochemical experimental set up is shown in Fig. 1~~x~~. The electrochemical techniques utilized in this project were anodic polarization, OCP, and the galvanostatic hold. The OCP and anodic polarization techniques were used to characterize the potential and anodic kinetics of the coating, whereas the galvanostatic hold was the method for selective dissolution.

OCP

The OCP technique measured the potential of the sample's surface in 0.6 M NaCl. The experimental set up for this technique can be seen in Fig. ~~x+1~~2. The OCP value is critical to establish the electrochemical potential of the sample before and after the selective dissolution technique, as the potential of the sample directly relates to its reactivity and nobility. Moreover, the OCP was measured to see whether the galvanostatic hold allows for the potential to be within the SCC immunity region of -0.7 V vs. SCE to -0.3 Volts (V) vs. Saturated Calomel Electrode (SCE). This project's electrochemical results were measured versus a Siver/Silver Chloride electrode for the sake of solution compatibility, but the values were converted to versus SCE to ensure that it is comparable to the immunity potential region. The duration of the OCP technique varies from five minutes up to an hour until the potential measurement stabilizes around the centivolt value as that is the stabilization criteria for purposes of this project.

Anodic Polarization

Anodic polarization in the DIPSOL IZ-C17+ solution provided insight into the anodic corrosion kinetics of the Zn-Ni coating on the steel substrate. The technique exposes the sample to a range of potentials that are above its measured OCP, to identify a viable current density range for the optimization of the selective dissolution process.

Galvanostatic Hold

The galvanostatic hold is the foundation of the selective dissolution process. This technique imparts a specified current onto the working electrode for a designated time or until the measured potential of the sample reaches a designated limit. The set up for the galvanostatic technique can be seen in Fig. 3~~X+2~~. This technique is parameterized for the targeted dissolution by adjusting the amount of current imparted, which is in the range of current densities of 1 mA/cm^2 up to 100 mA/cm^2, for the scope of this project. A duration of a 30-minute limit was the original benchmark but was later replaced with a potential limit of 0.5 V vs. SCE. The 30-minute limit was established to keep the post-processing to be within the same magnitude of time as the electrodeposition process employed by TechMetals. The time limit was no longer relevant when it became clear that the potential limit allowed for greater control over the amount of selective dissolution, which was important once the 10 mA/cm^2 current density appeared to be the most favorable for the selective dissolution process.

Characterization Methods

XRD

Prior to electrochemical experimentation, a sample from batch 3 and batch 4 underwent XRD characterization, housed in UVA NMCF, to better understand the crystal structure as a product of the original coating processing. Moreover, this data was used to confirm the composition of the coating by comparing the diffraction patterns produced by XRD to the identification cards in the HighScore database. Included below is a diffraction pattern with the matching peaks to an identification card to give insight into the coating processing, all diffraction patterns across batches were similar and thus, this data is widely representative.

SEM

The samples used for analysis were selected as standards and particular points of interest, such as samples that had reached the desired potential range. Samples were characterized in plan and/or cross-sectional views. Cross-section samples were sectioned, mounted in epoxy, and sputter coated with Au-Pd using the Cressington Sputter Coater housed by UVA NMCF. Each sample was secured to an appropriate platen with carbon tape. For all back-scattered electron (BSE) micrographs unless otherwise noted, the concentric backscatter (CBS) detector was used with the rings A, B, and sometimes C, which produces a compositional contrasted micrograph. The rings allow for a separation of signal by emittance angle. The A ring captures the most amount of compositional information and the least amount of topographical information. With each subsequent ring, the amount of compositional information decreases and the topographical amount of information increases. For the imaging purposes in this report, the rings were selected to provide the best contrast and most relevant information. Relevant micrographs to display the progression of this project are shown below. Due to time constraints, not all samples available or tested were characterized under SEM. The samples that were tested and not further characterized include B3-R10, B3-R12, B3-R7, and B3-R8.

Energy Dispersive Spectroscopy (EDS)

All quantitative EDS analysis was performed on samples in plan view and are subject to increased skepticism on the quantitative nature of the data because of penetration depth of the electron beam interacting with the variable surface roughness of the samples. This is because the surface roughness can alter the signal received with increased or decreased absorption based on the features next to the point of interest as the distance to the surface will change with neighboring peaks and valleys. In addition, the surface depth of EDS ranges from 300-5000nm below the surface. At the thinnest points of the film, especially after treatment, this could penetrate through the residual coating, picking up more substrate signal instead. This is not considered an issue with EDS on a polished surface, such as in cross-section. EDS scans were performed in point, line, and map mode, with greater emphasis on line scans.

Detailed Drawings

Electrochemical Set Up

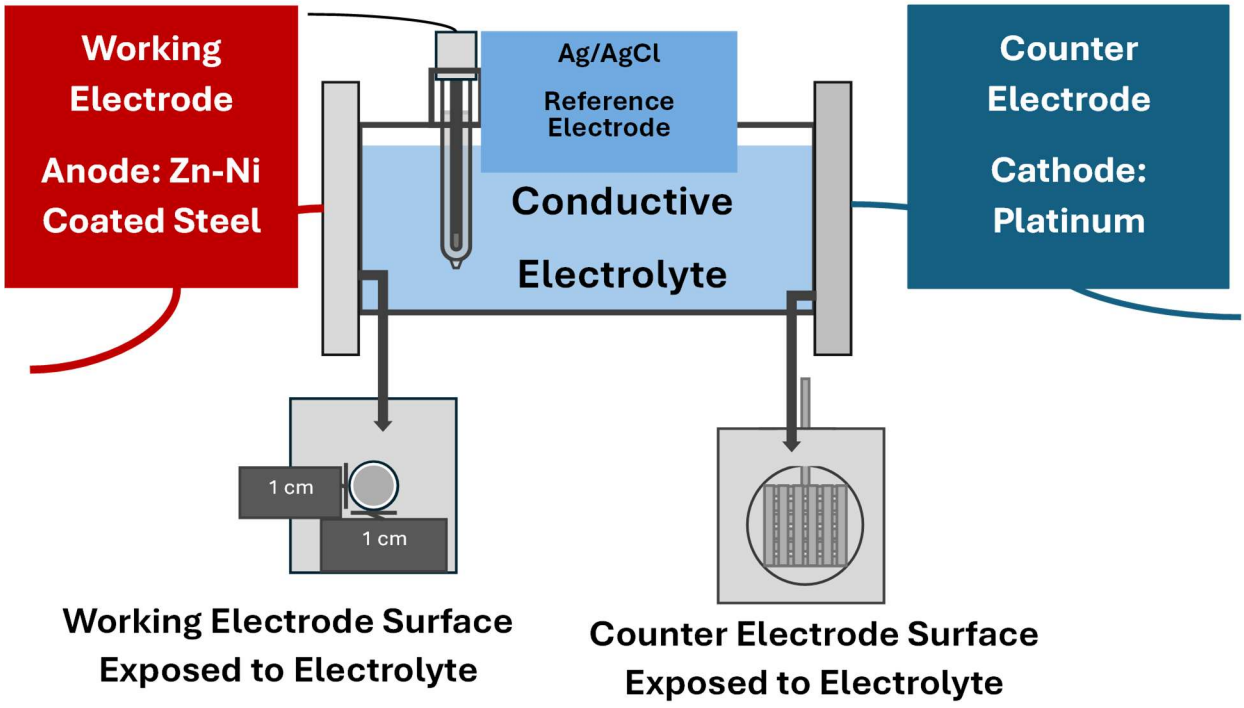

Fig. 1. Electrochemical cell experimental set up and components, with a view of the exposed sample surface area.

Open Circuit Potential Technique

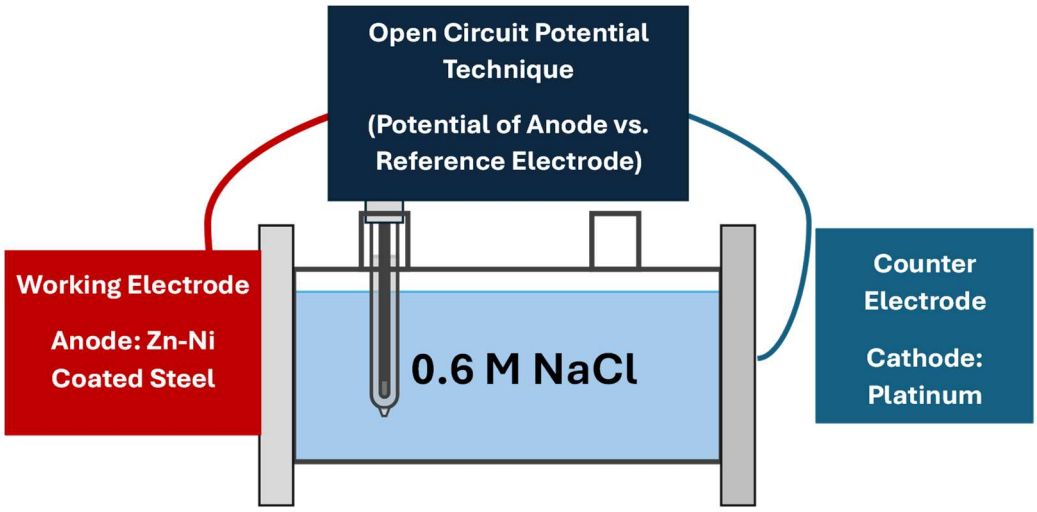

Fig. 2. The experimental set up of the Open Circuit Potential technique and the relevant electrodes.

Galvanostatic Technique

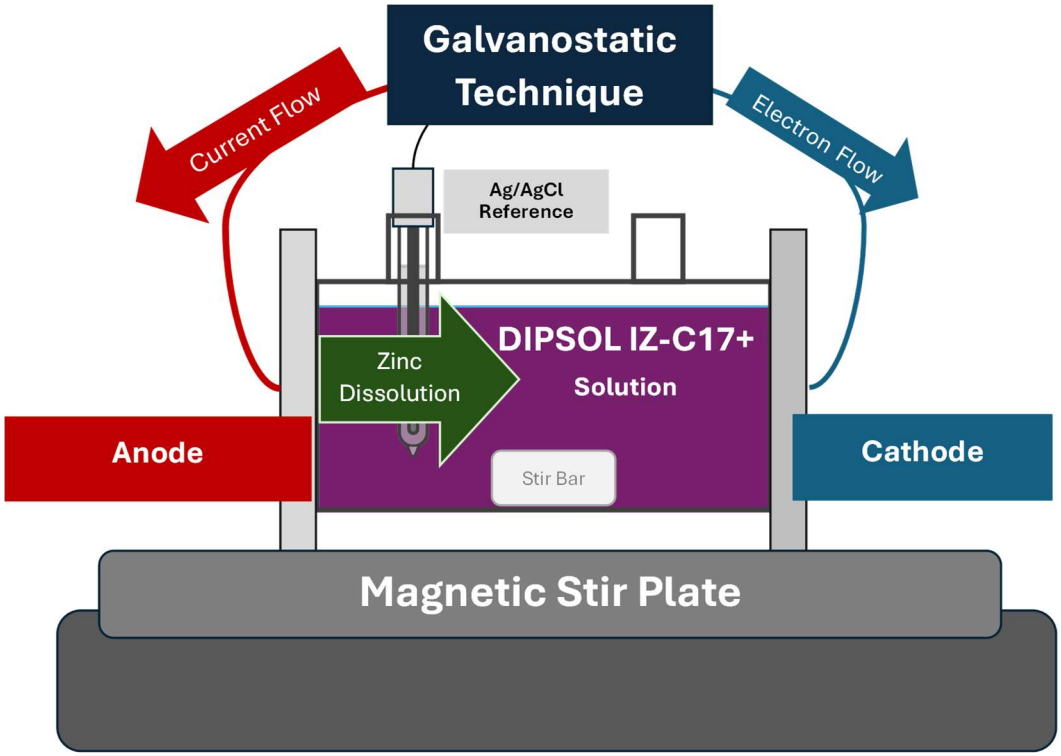

Fig. 3. The galvanostatic technique's experimental set up, current flow and electron flow direction, and the relevant electrodes.

Results: Characterization and Analysis

Below is an overview of the electrochemical experimentation performed in chronological order with the associated current densities and times performed, as well as the OCP before and after the selective dissolution technique. XRD characterization was used to identify the structural information of the as-received samples. Finally, the major findings from SEM and EDS characterization are shown to highlight how the Zn-Ni coatings were altered.

Electrochemical

Electrochemical Results Summary

The electrochemical experimentation optimized the parameters for a selective dissolution technique that would preferentially target and dissolve the Zn out of the Zn-Ni electrodeposited coating. The technique would enrich the surface of the coating with Ni and increase the nobility of the coating to be within the immunity potential region of -0.7 V vs. SCE to -0.3 V vs. SCE. The first attempts explored the 1-100 mA/cm^2 range of current densities for a time of 30 minutes to determine the current density which would be within the time constraint and potential change constraint. The time limit was excluded from the following experimental constraints and was replaced by a potential limit that was first -0.5 V vs. SCE and then lowered to -0.7 V vs. SCE, as the higher limit enhanced the risk of coating removal. However, the immunity potential region was only achieved with an added step of 20-minute stirring portion to the OCP technique that took place after the galvanostatic technique. The stirring had a continued effect on the OCP of the sample even after stirring had stopped, which led to multiple batch 3 samples to successfully reach the potential immunity region, as well as a batch 4 sample.

Table 3. A complete table of the parameters and the results associated with the electrochemical tests that were completed for the optimization of the selective dissolution technique.

R = Regular Sample *Appendix A: label nomenclature			Experimentation						
Sample Label*	Bag	Number	Date	OCP Before (V vs. SCE)	Current Density (mA/cm^2)	Potential Limit (V Vs. SCE)	Time (mins)	OCP After (V vs. SCE)	OCP After Stir (V vs. SCE)
B3-R5	3	5	1/30/2024	-0.980	1	N/A	30	-0.931	N/A
B3-R9	3	9	2/2/2024	-0.972	10	N/A	30	-0.93	N/A
B3-R10	3	10	2/10/2024	-0.965	100	N/A	30	-0.799	N/A
B3-R11	3	11	2/15/2024	-0.985	100	N/A	30	-0.86	N/A
B3-R12	3	12	2/19/2024	-0.977	150	N/A	30	-0.91	N/A
B3-R23	**3**	**23**	**2/19/2024**	**-0.972**	**10**	**N/A**	**62**	**-0.92**	**-0.601**
B3-R20	**3**	**20**	**2/25/2024**	**-0.971**	**10**	**-0.5**	**45**	**-0.862**	**-0.61**
B3-R7	3	7	3/6/2024	-0.972	100	-0.5	5.15	-0.705	-0.73
B4-R2	**4**	**2**	**3/12/2024**	**-0.825**	**10**	-0.5	**42**	**-0.55**	**-0.568**
B3-R8	**3**	**8**	**3/19/2024**	**-0.978**	**10**	**-0.5**	**45**	**-0.6**	**-0.56**
B3-R28	**3**	**28**	**4/2/2024**	**-0.985**	**10**	**-0.7**	**85**	**N/A**	**-0.58**

The bolded rows indicate the samples that reached the immunity potential region.

Table 4. Legend for electrochemical graphs

Blue Background =	**Tests done in 0.6 M NaCl**
Dark Purple Background =	**Tests done in DIPSOL IZ-C17+**
Green Highlight =	**Immunity Potential region reached!** (-0.7 V vs. -0.3 V)
Rust Highlight =	**Periods of Active Stirring**

Current Density Range and 30 Minute Time Limit

The current density range of interest was 1-100 mA/cm^2, as previous work done by Victor Kontopanos indicated that 1 mA/cm^2 was able to successfully reach the immunity potential region. This was achieved through multiple exposures of 20 minutes each in the 0.6 M NaCl. The selective dissolution technique for this project would be for a single exposure time and the solution would be the existing plating solution, DIPSOL IZ-C17+. Sample B3-R5 was exposed to 1 mA/cm^2, sample B3-R16 was exposed to 10 mA/cm^2, and lastly, sample B3-R16 was exposed to 100 mA/cm^2, all with a 30-minute exposure time. For these tests, none of the samples had a measured OCP reach the immunity potential region, indicating that the 30-minute time limit was not sufficient and that a potential limit acted as a better benchmark during the galvanostatic hold. However, these tests also indicated that the 10 mA/cm^2 current density would be of greater interest, because of the constraint to selectively dissolve the Zn in the Zn-Ni matrix within a reasonable time.

In Fig. 4, the blue line shows the impact of the 1 mA/cm^2 galvanostatic hold on the B3-R5 sample in DIPSOL IZ-C17+ solution, with its OCP measured before and after in 0.6 M NaCl. The change in potential due to the selective dissolution technique was an increase of 49 mV. The orange line shows the impact of the 10 mA/cm^2 galvanostatic hold on the B3-R9 sample in DIPSOL IZ-C17+ solution, with its OCP measured before and after in 0.6 M NaCl. The change in potential due to the selective dissolution technique was an increase of 42 mV. The change in potential is less than the one seen with B3-R5, but the 10 mA/cm^2 galvanostatic hold, seen in Fig. 4~~X~~B indicated with an orange line, had a favorable linear potential region that will be explored in the next section. The dark yellow line indicated in Fig. 4 shows the impact on the OCP of B3-R11 due to a galvanostatic hold of 100 mA/cm^2 for 30 minutes. A change of potential of 158 mV was measured when testing the 100 mA/cm^2 electrochemical condition, which is expected as this was the upper limit of the current range candidates for optimization. The magnitude of this potential change required further exploration by expanding the study to include an additional 30-minute exposure to B3-R11 at the same current density to explore the magnitude of potential change for a total exposure.

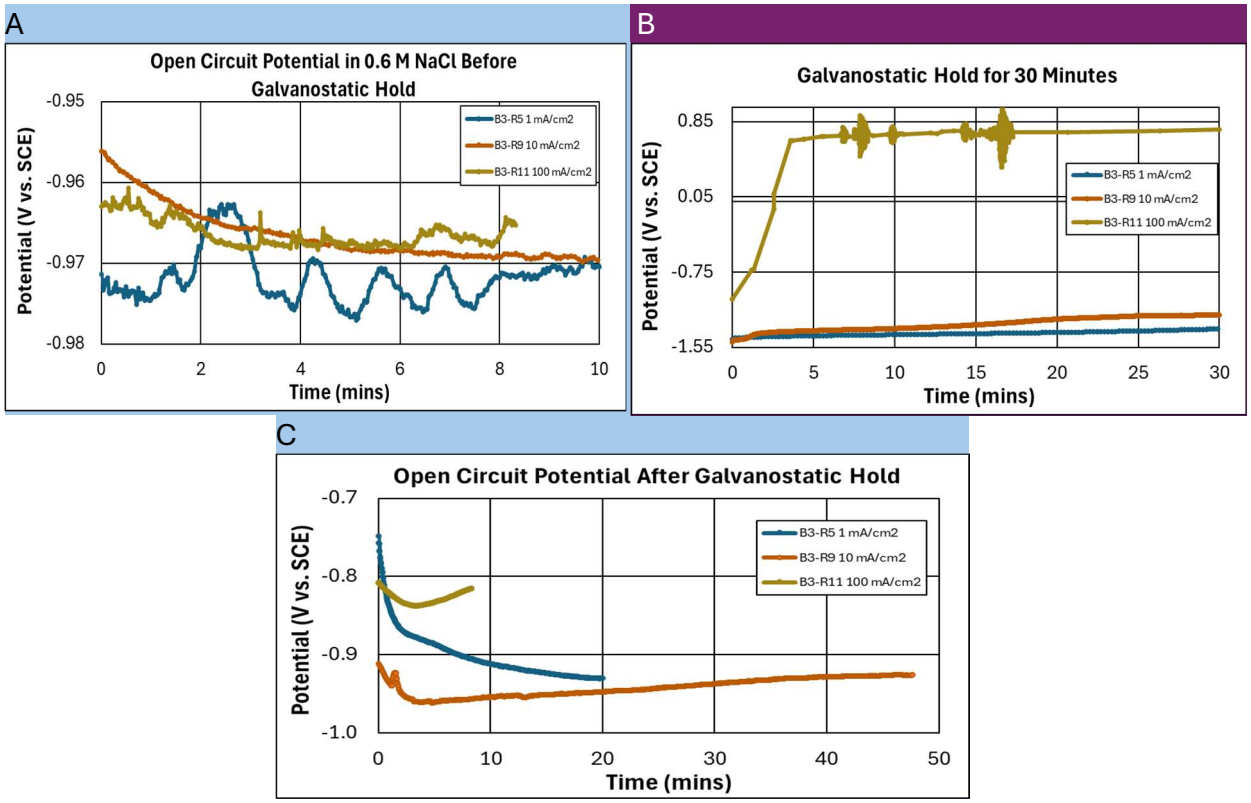

Fig. 4. A) OCP of sample B3-R5, blue line, sample B3-R16, orange line, and sample B3-R11, dark yellow line. B) Galvanostatic hold of 1 mA/cm^2 on sample B3-R5, blue line. Galvanostatic hold of 10 mA/cm^2 on sample B3-R16, orange line. Galvanostatic hold of 100 mA/cm^2 on sample B3-R11, dark yellow line. C) OCP after galvanostatic hold, of sample B3-R5, blue line, sample B3-R16, orange line, and sample B3-R11, dark yellow line.

As represented by the dark yellow line in Fig. 5, the impact on the OCP of B3-R11 due to a galvanostatic hold of 100 mA/cm^2 for 30 minutes can be understood. This is coupled with the electrochemical results of a subsequent second exposure, indicated by the green line in Fig. 5. A change in potential of 158 mV was measured during the first exposure, which is expected as this was the upper limit of the current range candidates for optimization. However, the increase in the potential of the sample was not recorded for the second exposure. After a subsequent 30-minute galvanostatic hold at 100 mA/cm^2, the OCP recorded was lower than the OCP measured after the first exposure. Compared to the baseline OCP of the sample, the change in potential was only 128 mV after the second exposure.

Blue Background =	Tests done in 0.6 M NaCl
Dark Purple Background =	Tests done in DIPSOL IZ-C17+

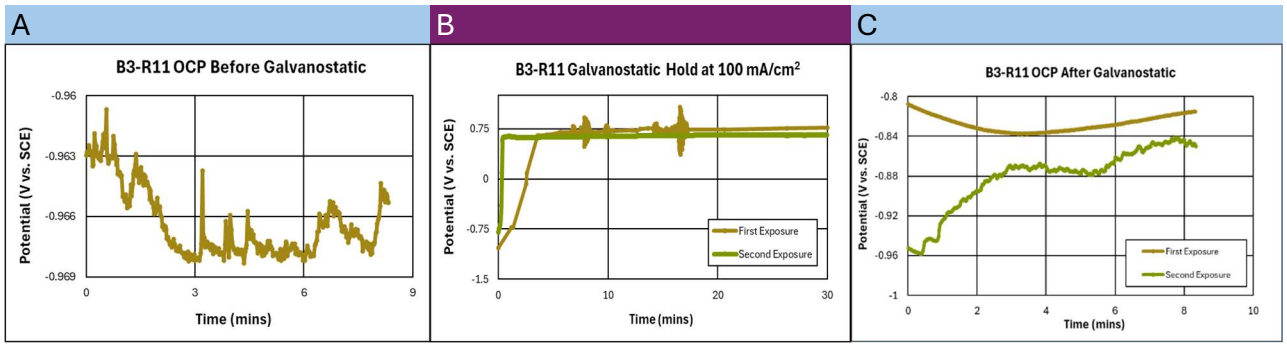

Fig. 5. Sample B3-R11 A) OCP in 0.6 M NaCl before galvanostatic hold; B) The change in potential due to the galvanostatic hold of 1 mA/cm2 for thirty minutes in DIPSOL IZ-C17+, with repeated exposures; C) OCP in 0.6 M NaCl after the first and second galvanostatic hold.

-0.5 V vs. SCE Potential Limit and the Addition of Stirring in 0.6 M NaCl

As explained in the previous section, the 10 mA/cm^2 current density was chosen to optimize the selective dissolution of Zn from a Zn-Ni electrodeposited coating. Sample B3-R3 was exposed to the current density for a one-hour period. The purpose of this test was to display the relationship between longer exposure durations, the upper range of the time constraint, and OCP of the sample at the. However, sample B3-R3 did not reach the immunity potential region until an additional stirring condition was engaged at 900 RPM for 20 minutes during the last OCP portion in 0.6 M NaCl. The stirring had a permanent effect on the OCP and increased the sample potential into the immunity region. Moreover, this test led to the establishment of a potential limit on galvanostatic hold that replaced the original design of a time limit. These procedure changes were repeated to determine the reliability of the technique on multiple batch 3 samples and a test on a batch 4 sample.

Fig. 6 shows the results of sample B3-R23 which underwent electrochemical exposure to 10 mA/cm^2 for approximately a one-hour period. This data clarifies the impact on OCP due to the selective dissolution technique. The change in potential before the stirring portion in the OCP after the galvanostatic hold was only 63 mV, but after the exposure to 20 minutes of stirring at 900 RPM, the change was 273 mV at the 50-minute mark, as seen in Fig 6C. The change in potential after 13 hours was measured to approximately be 350 mV, as seen in Fig. 6D. The potential of the samples stabilized around -630 mV, which is within the immunity potential region. Furthermore, the dramatic increase in potential around the 55-minute mark, as seen in Fig. 6B, was not favorable. Thus, a potential limit of -0.5 V vs. SCE was established for the remainder of the experimentation.

Blue Background =	Tests done in 0.6 M NaCl
Dark Purple Background =	Tests done in DIPSOL IZ-C17+
Green Highlight =	Immunity Potential region reached! (-0.7 V vs. -0.3 V)
Rust Highlight =	Periods of Active Stirring

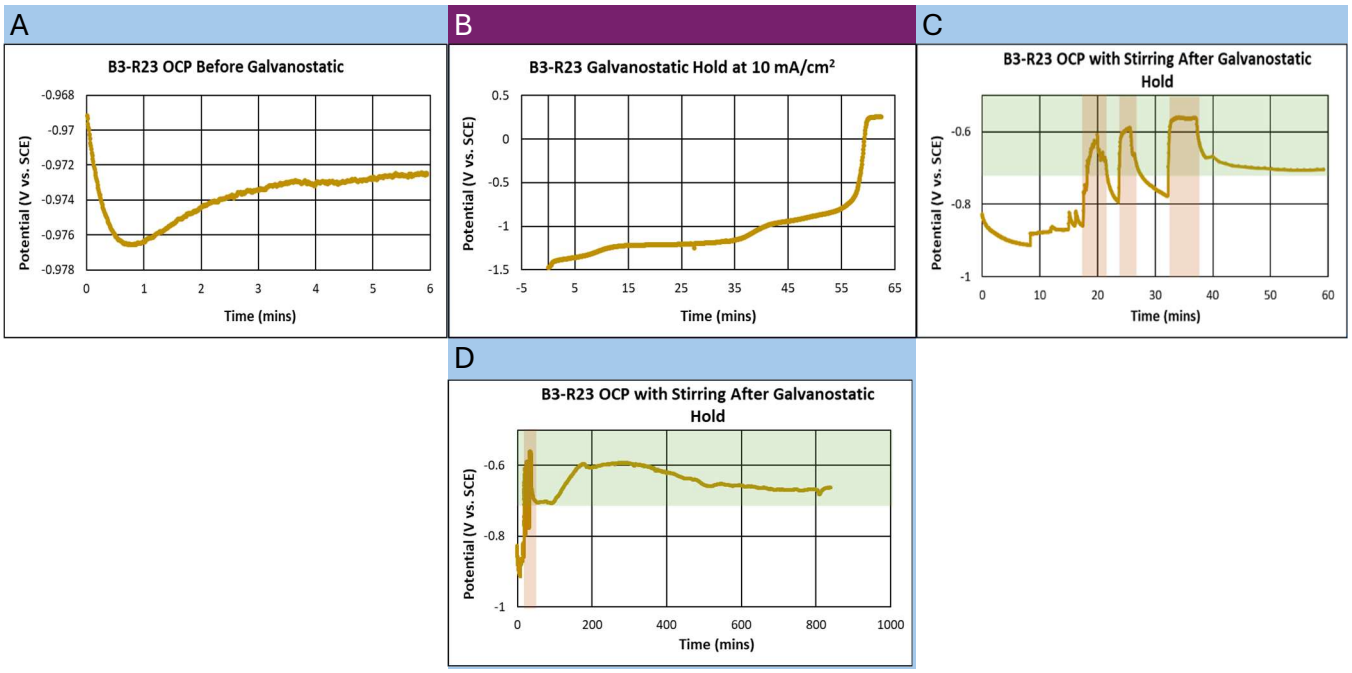

Fig. 6. Sample B3-R23 A) OCP in 0.6 M NaCl before galvanostatic hold; B) The change in potential due to the galvanostatic hold of 10 mA/cm2 for 62 minutes in DIPSOL IZ-C17+; C) The first 60 minutes of the OCP technique in 0.6 M NaCl, including the sections of stirring at 900 RPM; D) The extended view of the 13 hour long OCP technique to test the impact of stirring in the 0.6 M NaCl after the galvanostatic technique.

Fig. 7 displays sample B3-R20 and baseline OCP, the galvanostatic hold of 10 mA/cm^2, and the relative impact of the galvanostatic hold on the OCP of the sample. Furthermore, this data shows the contribution of stirring in the 0.6 M NaCl during the OCP test. The end of the galvanostatic hold was set to be when the potential of the sample reached -0.5 V vs. SCE in the DIPSOL IZ-C17+. This was established due to the galvanostatic behavior of B3-R23, as the change in the potential of the sample dramatically increased once it reached the -0.5 V vs. SCE value. The change in potential was 100 mV before the stirring portion. The change dramatically increased once the stirring ceased and the OCP stabilized, with the increase of 370 mV. This brought the sample into the immunity potential region.

Blue Background =	Tests done in 0.6 M NaCl
Dark Purple Background =	Tests done in DIPSOL IZ-C17+
Green Highlight =	Immunity Potential region reached! (-0.7 V vs. -0.3 V)
Rust Highlight =	Periods of Active Stirring

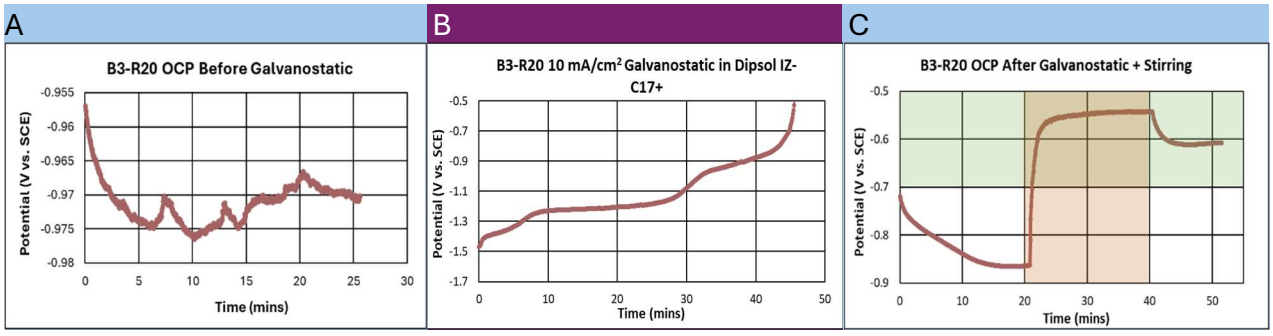

Fig. 7. Sample B3-R20 A) OCP in 0.6 M NaCl before galvanostatic hold; B) Change in potential due to the galvanostatic hold of 10 mA/cm2 until the 0.5 V vs. SCE potential limit in DIPSOL IZ-C17+; C) OCP in 0.6 M NaCl, with 20 minutes of stirring, after the galvanostatic hold.

Fig. 8 shows the OCP of sample B3-R8 before and after a galvanostatic hold of 10 mA/cm^2. There was an extreme change in potential, even before the addition of stirring, with an increase of 368 mV. This increase was continued after the stirring portion had ceased and the OCP stabilized, with a total increase of 413 mV. This sample had that same potential limit established by the test above, stopping once the potential of the sample had reached -0.5 V vs. SCE in the DIPSOL IZ-C17+ solution. Sample B3-R8 was unique in that it reached the immunity region without the addition of stirring, which was not seen in any other batch 3 samples that had been exposed to 10 mA/cm^2.

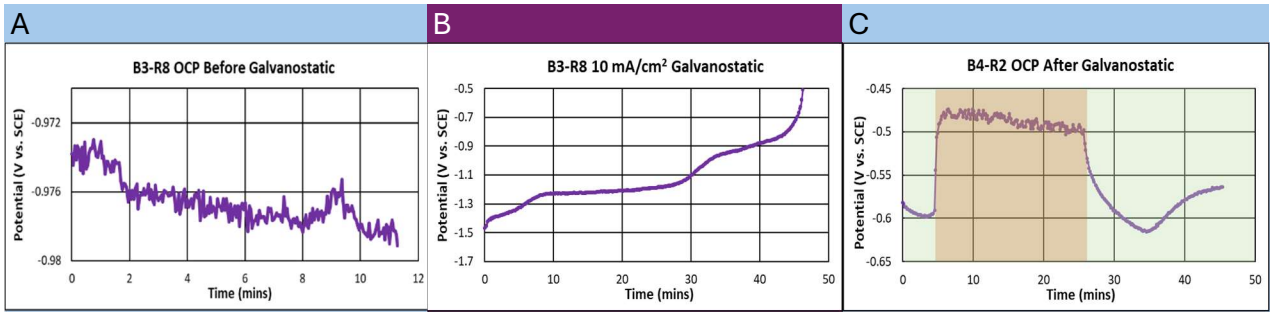

Fig. 8. Sample B3-R8 A) OCP in 0.6 M NaCl before galvanostatic hold; B) Change in potential due to the galvanostatic hold of 10 mA/cm2 until the 0.5 V vs. SCE potential limit in DIPSOL IZ-C17+; C) OCP in 0.6 M NaCl, with 20 minutes of stirring, after the galvanostatic hold.

Selective Dissolution Technique on Batch 4

Fig. 9 shows the effect of the selective dissolution technique on sample B4-R2. The baseline OCP was measured in 0.6 M NaCl, followed by the 10 mA/cm^2 galvanostatic hold technique until the potential of the sample reached -0.5 V vs. SCE. Then, OCP was measured in 0.6 M NaCl with a 20-minute stirring portion at 900 RPM which continued until the OCP stabilized. The batch 4 sample had a much higher starting OCP, of around -830 mV vs. SCE, so there was a lesser change in potential, but the sample was able to reach the immunity potential region. The overall change in potential of the sample was 260 mV, however the impact of stirring is questionable for sample B4-R2, because the measured OCP after the galvanostatic hold did not stabilize before the stirring was engaged. Thus, it is not clear whether the stirring had a noticeable impact on the OCP after it had ceased.

Blue Background =	Tests done in 0.6 M NaCl
Dark Purple Background =	Tests done in DIPSOL IZ-C17+
Green Highlight =	Immunity Potential region reached! (-0.7 V vs. -0.3 V)
Rust Highlight =	Periods of Active Stirring

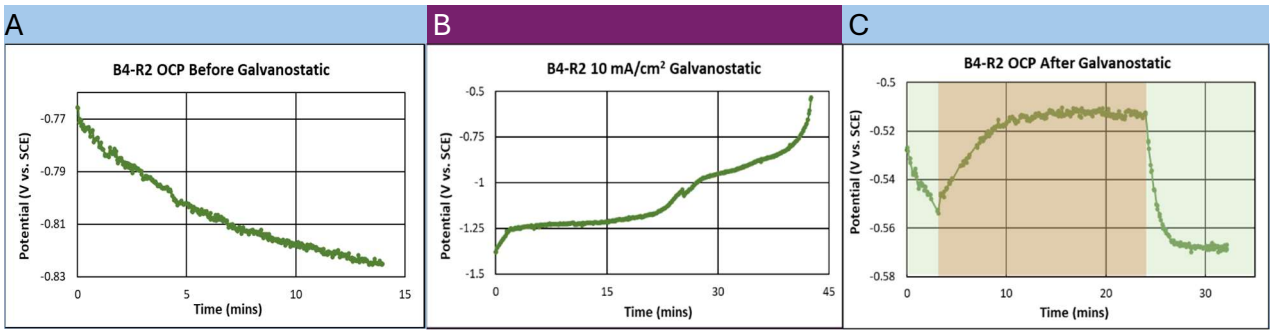

Fig. 9. Sample B4-R2 A) OCP in 0.6 M NaCl before galvanostatic hold; B) Change in potential due to the galvanostatic hold of 10 mA/cm2 until the 0.5 V vs. SCE potential limit in DIPSOL IZ-C17+; C) OCP in 0.6 M NaCl, with 20 minutes of stirring, after the galvanostatic hold.

-0.7 V vs. SCE Potential Limit Instead of -0.5 V vs. SCE Potential Limit

SEM characterization on the samples that successfully reached the immunity potential region under the operating condition of -0.5 V vs. SCE potential limit displayed that most of the coating was no longer present on the substrate. This will be shown in the SEM results below this section. To prevent excessive dissolution, a lower potential limit of -0.7 V vs. SCE was adopted.

Sample B3-R28, as seen in Fig. 10, underwent the same procedure as the previous samples that had the experimental design including potential limit galvanostatic hold and 20-minute stir in the 0.6 M NaCl. However, unlike previous experimentation, the potential limit for sample B3-R28 was lowered to -0.7 V vs. SCE instead of -0.5 V vs. SCE. The overall potential change was 405 mV, and the stabilized OCP after stirring was within the immunity potential range. As seen in Fig. 10C, there is a missing portion of the data due to a premature wait technique, so the portion of missing data is represented with an orange bar. This was not critical, as the OCP change while actively stirring is not as important as the OCP measured once the stirring has ceased.

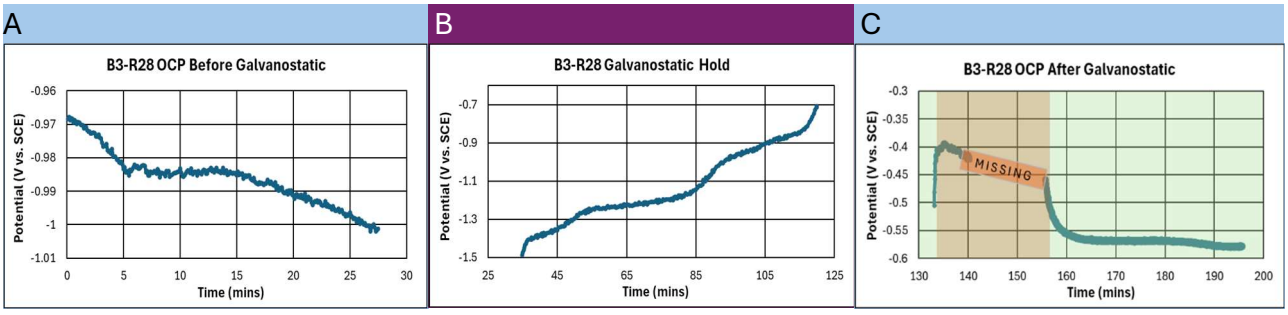

Fig. 10. Sample B3-R28 A) OCP in 0.6 M NaCl before galvanostatic hold; B) Change in potential due to the galvanostatic hold of 10 mA/cm2 until the 0.7 V vs. SCE potential limit

in DIPSOL IZ-C17+; C) OCP in 0.6 M NaCl, with 20 minutes of stirring, after the galvanostatic hold.

Pre-Characterization on Batch 3 and Batch 4 Samples

Sample B3-R5 displays the geometry and processing of the coating deposition which clarifies how that affects its selective dissolution properties. Below, in Fig. 11, it is apparent that the samples have a dendritic appearance. This is typical in plating and was further affirmed below in Fig. 12. which displays the diffraction pattern rendered from powder XRD (p-XRD). In this, it is evident that there is one diffraction peak, which represents a crystal orientation, which is preferred for growth after nucleation. The relative intensity of this peak indicates favor towards this one grain orientation. This is a characteristic of electrochemical coating.

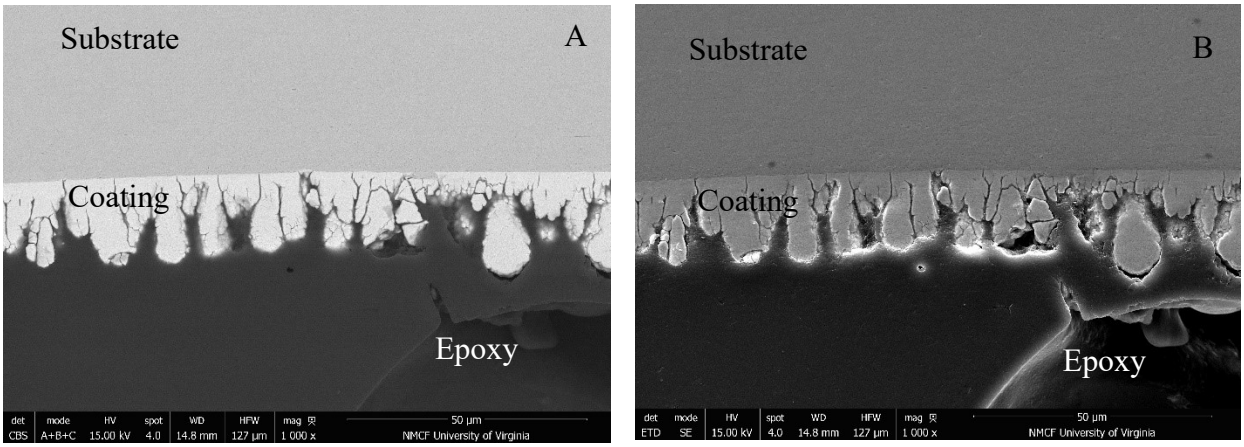

Fig. 11. Sample B3-R5 displays the columnar structure that is a characteristic of a coating applied by electrochemical deposition, seen in A) BSE micrograph and B) SE micrograph.

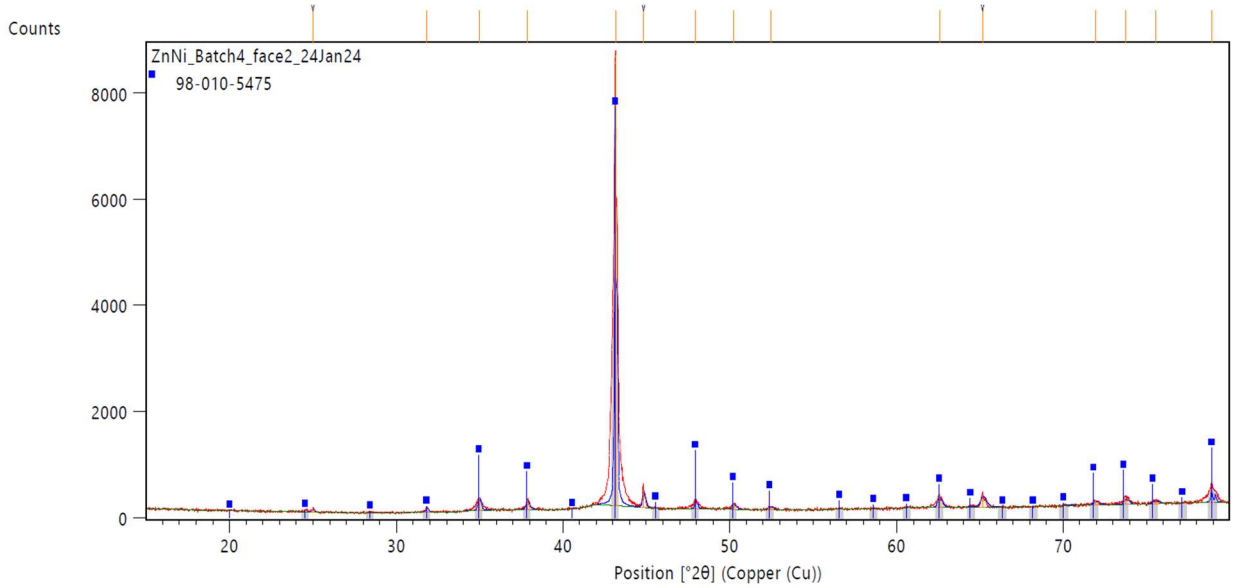

Fig. 12. As-received sample from B4 shows one strong diffraction peak which further supports that there is a preferential growth direction which is typical of electrochemical deposition.

Fig. 13 displays the cross section of the Zn-Ni coating present on sample B3-R2 and contains both a SE micrograph (a) and a BSE micrograph (b). The SE micrograph clearly exhibits the coating against the mounting epoxy, which is represented by the black region to the left of the coating line, and the substrate, which is represented by the grey region to the right of the coating line. The coating morphology is shown to be variable in thickness and geometry along the deposition area on the substrate. The BSE micrograph displays the compositional variation between the coating, the epoxy, and the substrate.

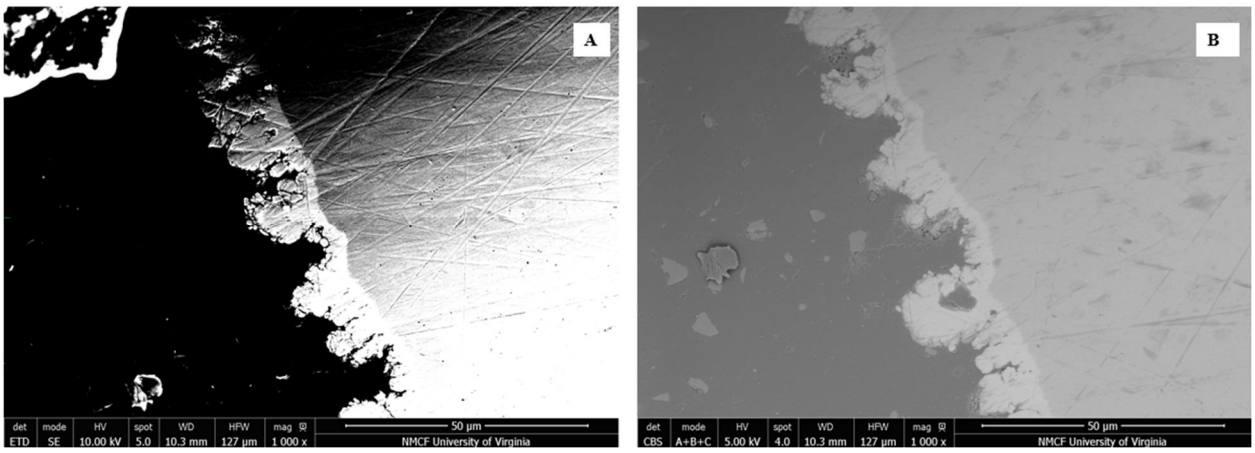

Fig. 13. Sample B3-R2 SEM micrographs: a) Zn-Ni coating cross section ETD at 1000x b) Zn-Ni coating cross section CBS at 1000x.

Fig. 14 contains both SE (A) and BSE (B) micrographs of the Zn-Ni coating on sample B3-R3. This region is characterized by a morphology of linear nodes. This result is consistent with the morphology observed on the coating of other samples. Fig. 15 consists of both SE (A) and BSE (B) micrographs of a cracked node found on sample B3-R3. These micrographs are included to provide a general morphological expectation for the coating structure at the deposition region on the substrate, which is dendritic, as well as a general morphological expectation for the coating on the face of the sample. Fig. 14 provides an expected morphology of the coating and serves as a point of reference for other samples presented in the section. Fig. 15 is included to display the possible defects present in the Zn-Ni coating. A discussion regarding the possible mechanism inducing the crack in Fig. 15 is provided in a later section.

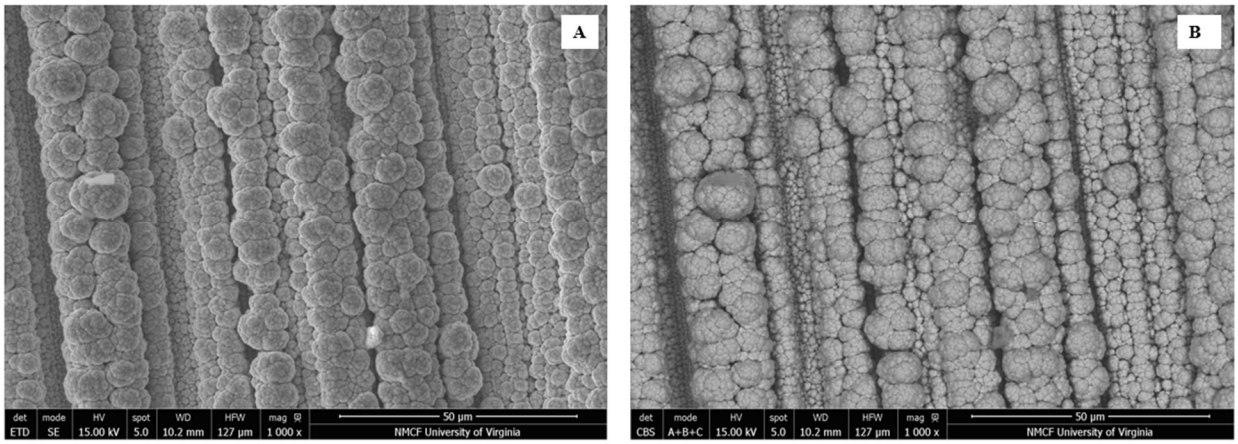

Fig. 14. Sample B3-R3 SEM micrographs: a) Zn-Ni coating ETD at 1000x b) Zn-Ni coating CBS at 1000x

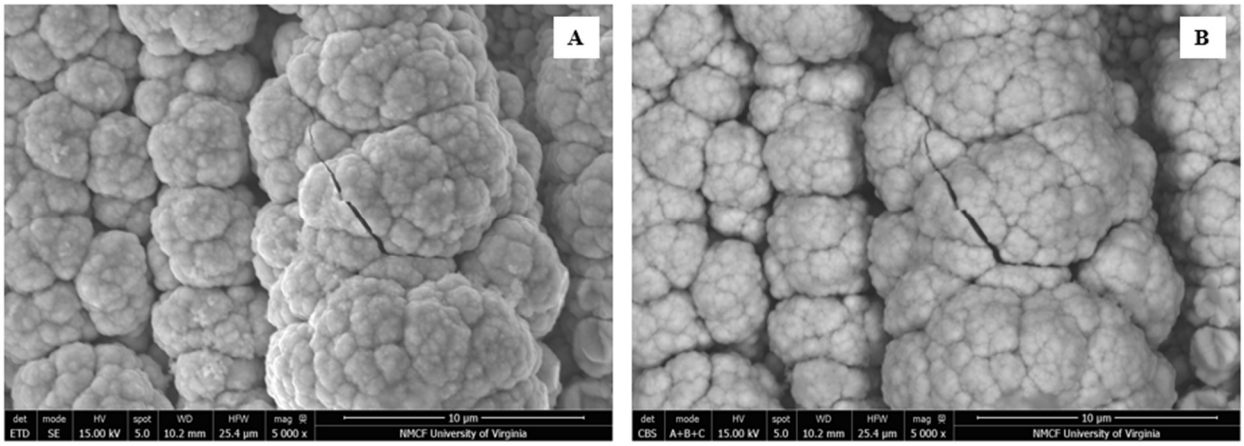

Fig. 15. Sample B3-R3 SEM micrographs: a) cracked node in Zn-Ni coating ETD at 5000x b) cracked node in Zn-Ni coating CBS at 5000x

Fig. 16 shows BSE micrographs in cross-sectional and plan view from batch 4. Fig. 16A shows the cross-section of sample B4-R3 where the thickest points of the coating were around 20µm. Fig. 16B shows sample B4-R12, which has more distributed nodes compared to the lines of nodes seen in batch 3.

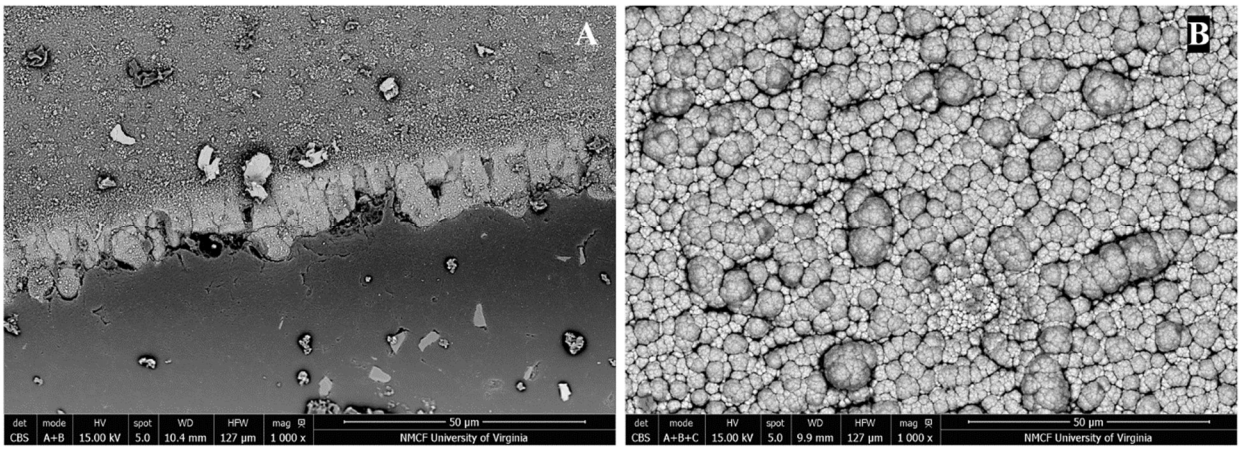

Fig. 16. A) Back-scattered electron (BSE) micrograph of B4-R3 at 1000x in cross-section. B) BSE micrograph of B4-R12 at 1000x in plan view.

Despite careful sample preparation, there appears to be a significant amount of particulate on the surface of several samples that could not be removed after several attempts. The samples affected are all cross-sections, including samples B3-R20, B3-R23, B4-R2, and B4-R3. The sputter coating would have been removed if any sample was wiped down, leaving the air gun as the only method for cleaning. The particulate was not macroscopically visible and putting it under vacuum to check proved time exhaustive. This contamination was not an issue in other cross-sectioned samples. It is unclear where the contamination was introduced and why it was such a problem for characterization for these samples. The particulate did obstruct several areas of interest but does not render micrographs or scans unusable. The primary objective for these cross-sections was the thickness of the coating.

Post-Characterization: 30 Minute Tests

One of the processing conditions changed to identify optimal processing parameters was duration. The duration of exposure was extended to a 30-minute period because shorter time periods did not remove a sufficient amount of Zn, and therefore the samples were not achieving an OCP in the immunity region. This can be seen below in Fig. 17 for sample B3-R5.

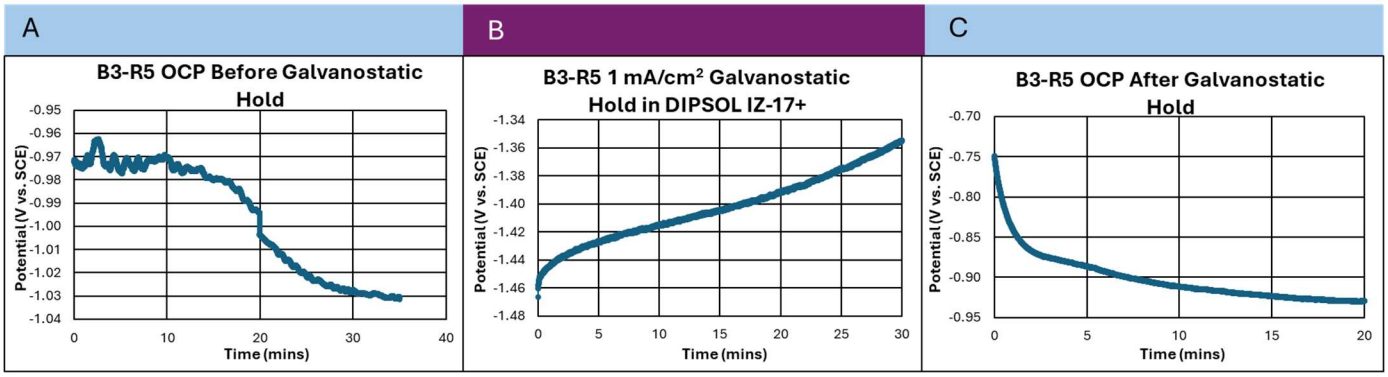

Fig. 17. Sample B3-R5 A) OCP in 0.6 M NaCl before galvanostatic hold; B) The change in potential due to the galvanostatic hold of 1 mA/cm2 for thirty minutes in DIPSOL IZ-C17+; C) OCP in 0.6 M NaCl after galvanostatic hold.

Fig. 17 shows the impact of the 1 mA/cm^2 galvanostatic hold on the B3-R5 sample in DIPSOL IZ-C17+ solution, with its OCP measured before and after in 0.6 M NaCl. The change in potential due to the selective dissolution technique was an increase of 49 mV. Despite this, cross-sectional microscopy, shown below in Fig. 18, elucidates that the coating is preserved throughout the electrochemical selective dissolution process.

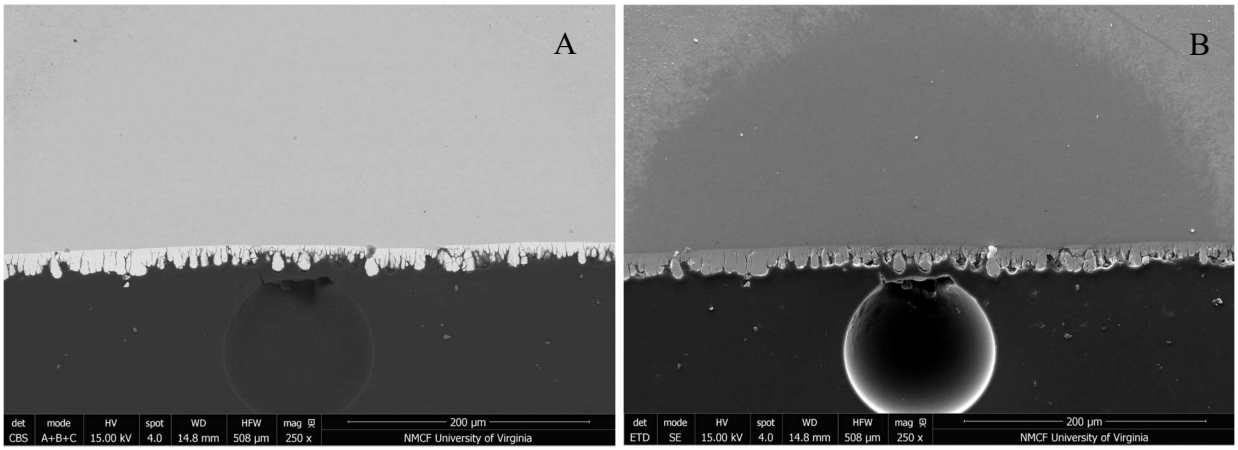

Fig. 18. Sample B3-R5 cross-sectional SEM micrographs display that the coating structure is consistent on the surface of the substrate after electrochemical selective dissolution technique A) BSE B) SE.

However, as seen in Fig. 19 below, plan view microscopy displayed that there is a change in the topography of the coating. The difference in brightness in this micrograph indicates a difference in relative height across the sample surface, which is due to the electrochemical selective dissolution of the coating.

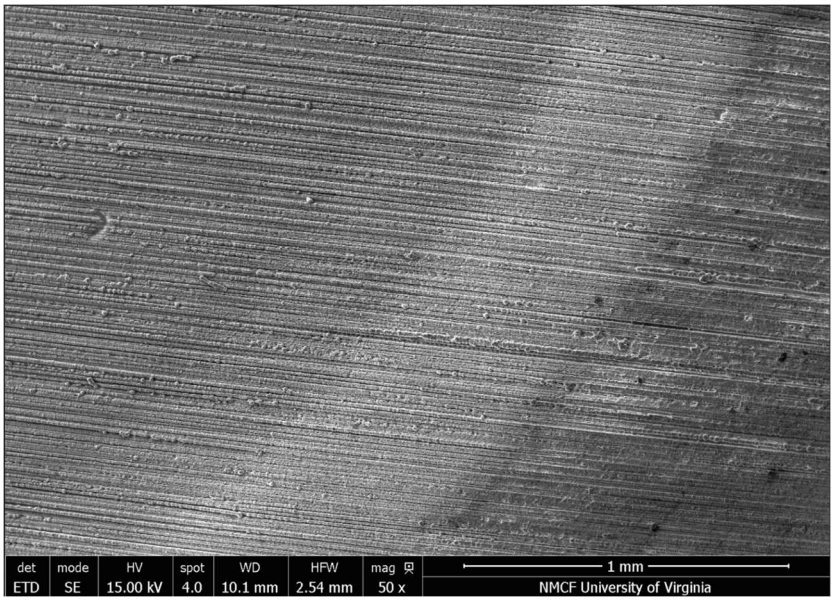

Fig. 19. Sample B3-R5 under plan view microscopy displays different relative distance from the electron detector based on the brightness captured in the micrograph.

The 30-minute exposure operating condition was also applied to sample B3-R9, as seen below in Fig. 20.

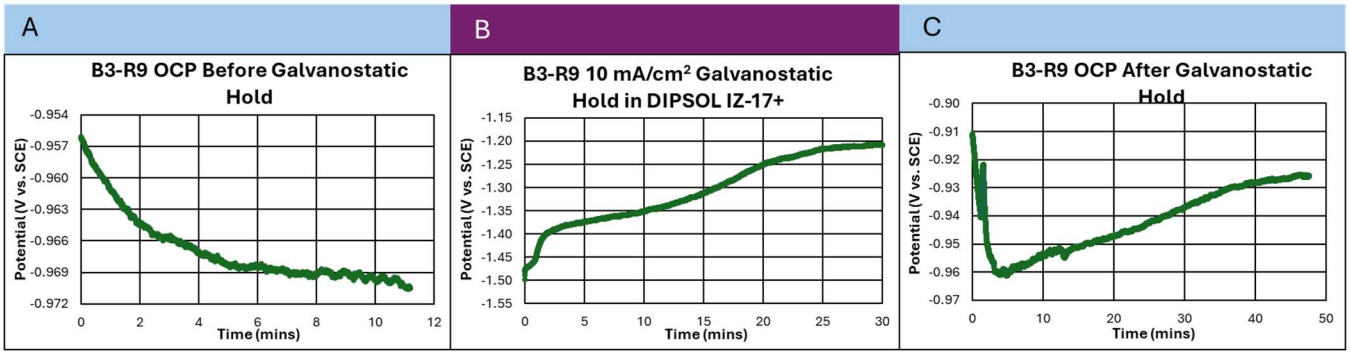

Fig. 20. Sample B3-R9 A) OCP in 0.6 M NaCl before galvanostatic hold; B) Change in potential due to the galvanostatic hold of 10 mA/cm2 for 30 minutes in DIPSOL IZ-C17+; C) OCP in 0.6 M NaCl after galvanostatic hold.

Fig. 20 shows the impact of the 10 mA/cm2 galvanostatic hold on the B3-R9 sample in DIPSOL IZ-C17+ solution, with its OCP measured before and after in 0.6 M NaCl. The change in potential due to the selective dissolution technique was an increase of 42 mV. The change in potential is less than the one seen with B3-R5, but the 10 mA/cm2 galvanostatic hold, seen in Fig. 5B, had a favorable linear potential region that could be explored in the next section.

These processing conditions did result in the coating on the sample to be electrochemically removed. This is evidenced by the difference between coating structure and

thickness as seen in Fig. 21. This is a series of cross-sectional micrographs which depict the coating structure and thickness after exposure to the selective dissolution technique, Fig. 21 A) compared to the unexposed face of the sample, Fig. 21 B). Both faces can be seen in Fig. 21 C), which clearly shows that the top side, unexposed face, is thicker and more consistent than the bottom side, the exposed face. Fig. 21 B) also shows that the coating maintained the columnar growth structure, whereas this is not present in Fig. 21 A).

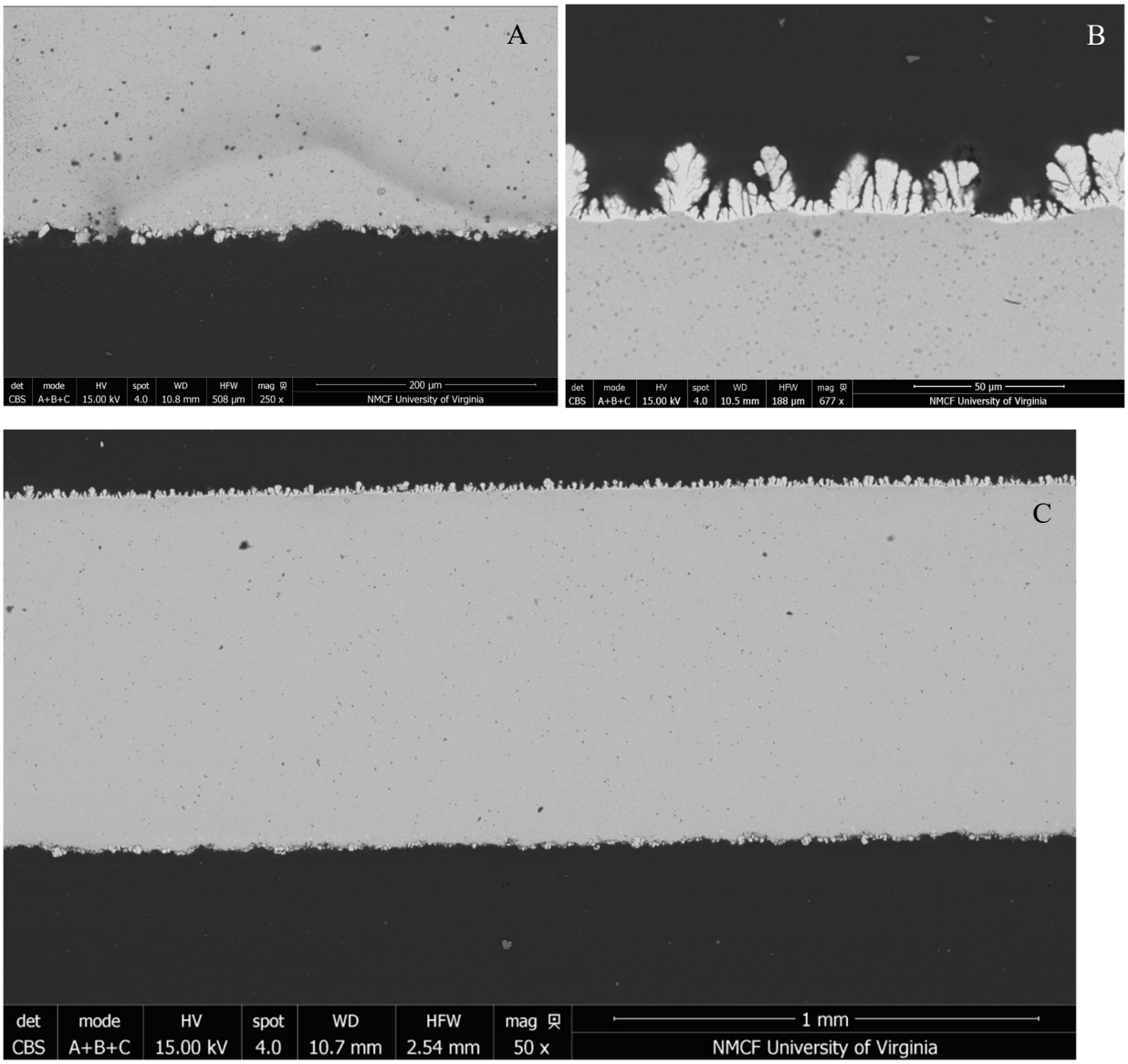

Fig. 21. displays SEM BSE cross-sectional micrographs for sample B3-R9 showing A) the face of the sample that was exposed to the electrochemical selective dissolution technique and B) the face of the sample that was unexposed and did not undergo this processing C) is a larger scale micrograph of the body of the sample which contrasts the coating of the thickness of both faces. The top side is the unexposed face and has a more apparent and thicker coating. Then, the bottom face is the exposed face with a thinner coating.

In Fig. 22, B3-R11 was characterized with electron microscopy after undergoing a second 30-minute exposure, which was preformed to study the potential change for a total exposure time of 60 minutes. Despite producing a change in potential of 158mV in the first exposure, the second exposure only altered the potential by 128 mV lower than the baseline OCP of the sample. This change is seen in Fig. 5.

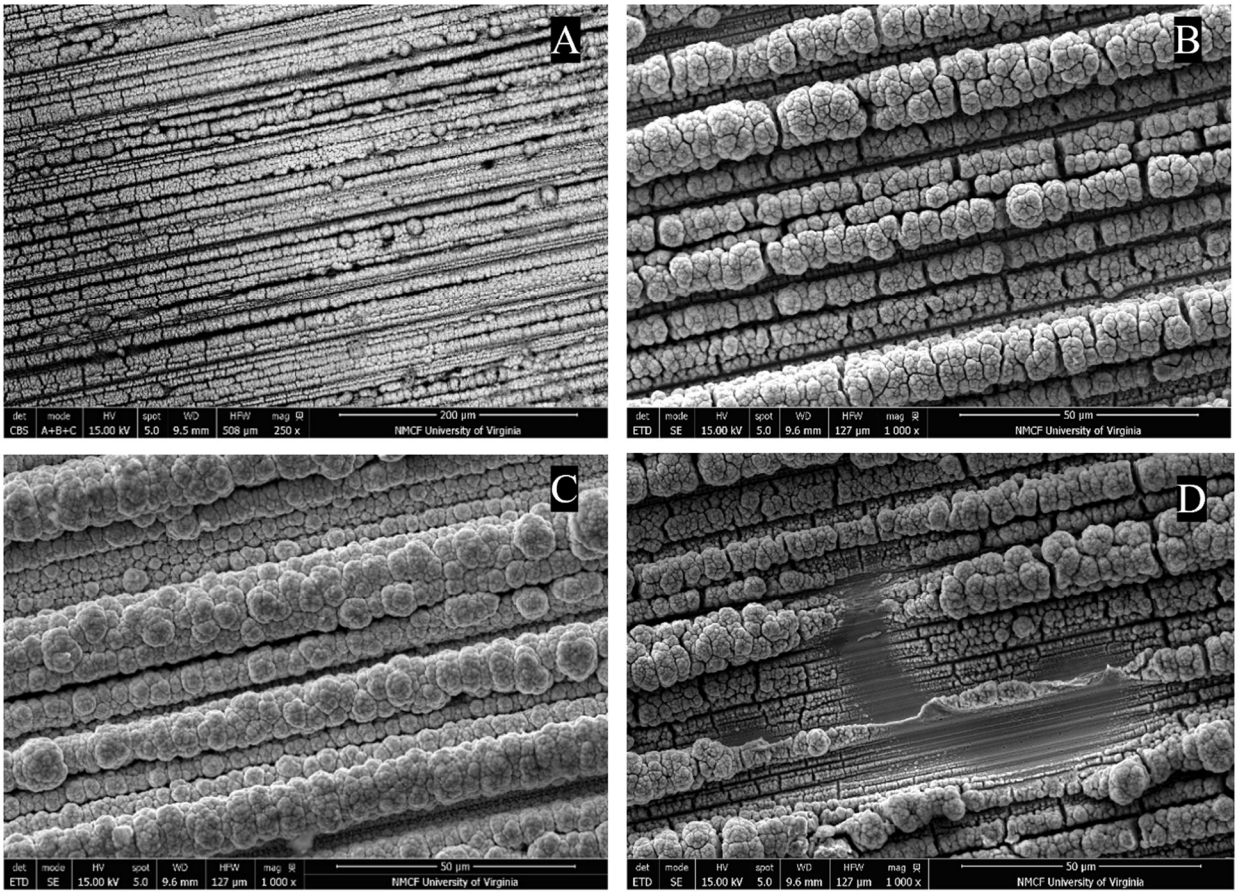

Fig. 22. A) BSE micrograph of B3-R11's the transition region from unexposed region to exposed region at 250x. B) SE micrograph of B3-R11's unexposed region at 1000x. C) SE micrograph of B3-R11's exposed region at 1000x. Secondary electron (SE) micrograph of point of interest on B3-R11 at 1000x. All micrographs are in plan view and done after the sample's second exposure.

The coating on B3-R11 maintained structural integrity for the most part post treatment. Within the surface area of the sample exposed to the selective dissolution, there are breaks in the lines of nodes that were not seen outside the affected area. This is apparent when comparing Fig. 22B and 22C. In addition, scattered thinning of the coating was seen. In these locations, the coating had been stripped to the surface as seen in Fig. 23 which shows EDS data. This data was used to qualitatively understand the present constituents on the surface of the sample. Though, there is high variability in the height of the surface which changes the quality and frequency of

the characteristic X-Rays detected. Thus, this data is only to show the variation in present constituents and not the relative ratio of composition.

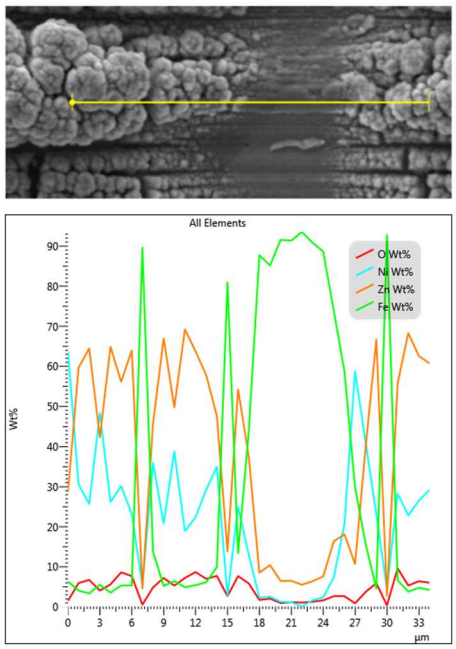

Fig. 23. EDS line scan of B3-R11 in planar view.

Post-Characterization: Batch 3 Samples with the -0.5 V vs. SCE Limit

Sample B3-23 underwent electrochemical exposure at 10mA/cm^2 for one hour, then stirring was introduced after a galvanostatic hold. This experiment, seen in Fig. 6, served to illustrate the impact of the selective dissolution on the OCP. This experimentation established the need for a potential limit of -0.5 V vs SCE. This limit was then used for sample B3-R20 in Fig. 7; moreover, this sample further exemplified the benefits of the galvanostatic hold on the OCP. Both B3-R20 and B3-R23 reached the immunity potential region; however, despite altered processing parameters, each displayed significant loss of coating within the area treated, as shown in Fig. 24.

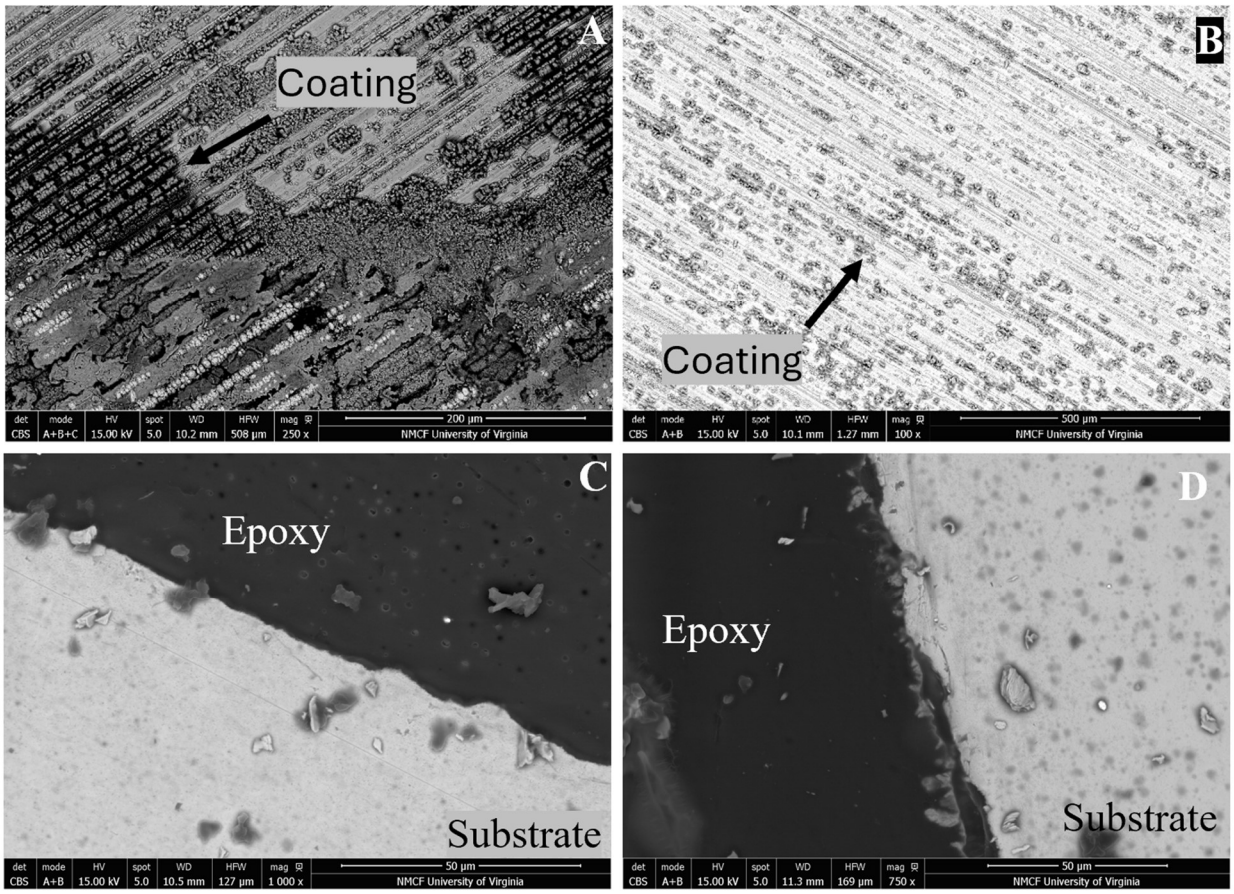

Fig. 24. A) BSE micrograph (CBS with ABC) of B3-R20 at 250x along edge of corrosion circle. B) B3-R23 plan view at 100x in the center of the corrosion circle. C) B3-R20 cross-section at 1000x. D) BSE micrograph of B3-R23 cross-section at 750x.

In plan view microscopy analysis, there is a small fraction of the original coating that remains. Fig. 24A demonstrates the protection of corrosive products along a point of contact with the gasket, allowing more coating to be retained compared to further away from the edges of the corrosion circle. The lighter background in Fig. 24B is the exposed substrate with the scattered darker lines being the coating that remained. This coating is thin enough for EDS signal to pass through to the substrate, shown in Fig. 25B. After sample preparation for cross-section microscopy, the coating could not be found and was not picked up in appreciable amounts with EDS, as seen in Fig. 25A.

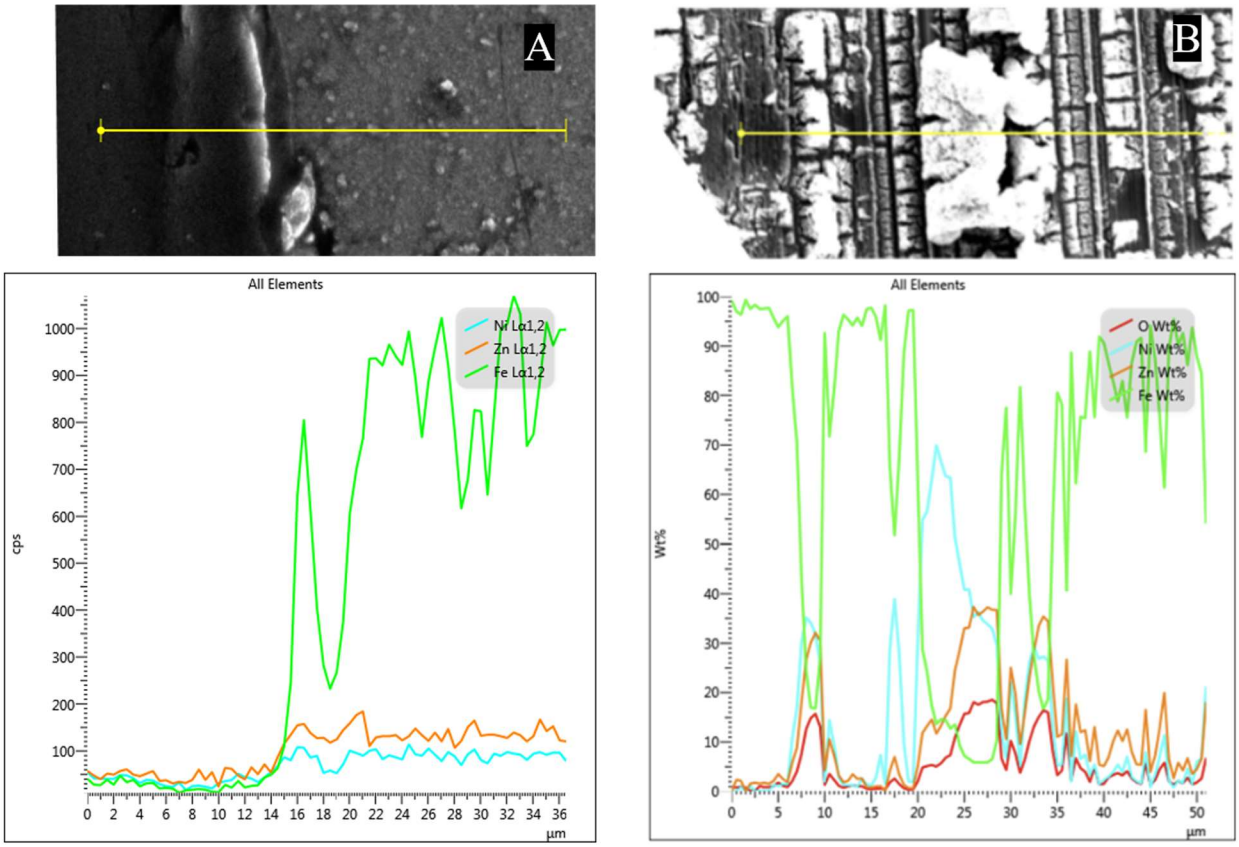

Fig. 25. A) EDS line scan of B3-R20 in cross-section. B) EDS line scan of B3-R23 in plan view.

B3-R8 also used a potential limit of -0.5 V vs SCE but was not characterized due to time constraints.

Post-Characterization: Batch 3 Sample with the -0.7 V vs. SCE Limit

Sample B3-R28, as seen in Fig. 26, underwent the same procedure as the previous samples who had the potential limit galvanostatic hold and 20-minute stir in the 0.6 M NaCl. However, B3-R28's potential limit was lowered to -0.7 V vs. SCE instead of -0.5 V vs. SCE. The overall potential change was 405 mV, and the stabilized OCP after stirring was within the immunity potential range. As seen in Fig. 26 C) there is a missing portion of the data due to a premature wait technique, so the portion of missing data is highlighted with an orange bar. This was not critical, as the OCP change while actively stirring is not as important as the OCP measured once the stirring has ceased.

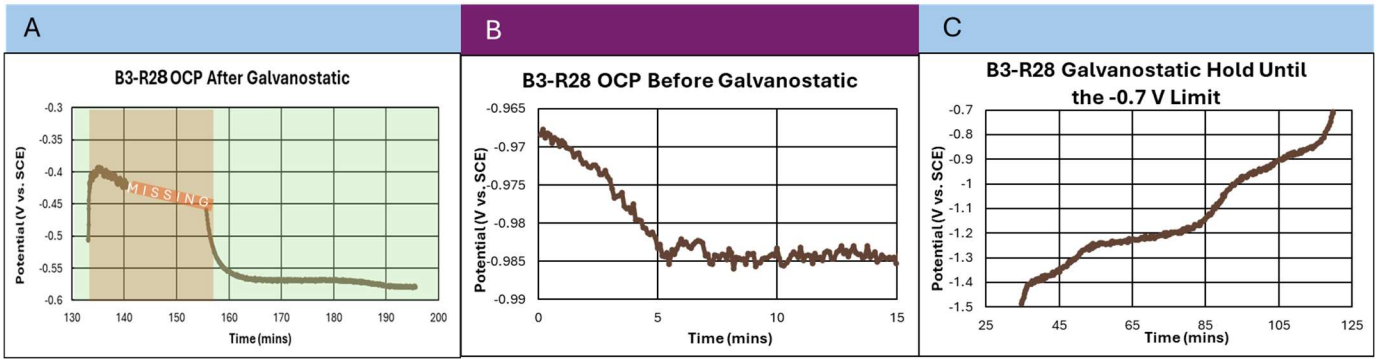

Fig. 26. Sample B3-R28 A) OCP in 0.6 M NaCl before galvanostatic hold; B) Change in potential due to the galvanostatic hold of 10 mA/cm2 until the 0.7 V vs. SCE potential limit in DIPSOL IZ-C17+; C) OCP in 0.6 M NaCl, with 20 minutes of stirring, after the galvanostatic hold.

As seen in Fig. 27, with the coating being completely stripped off from the sample substrate through electrochemical selective dissolution, the variation in coating presence can be seen dependent on whether the local surface was exposed or not. It is evident that toward the left side of the micrographs there is a thicker and more consistent coating compared to the right side and thus, it is deduced that somewhere within this frame exists the boundary between the exposed and unexposed surface. These micrographs clearly demonstrate that there originally was a robust coating present prior to selective dissolution, but the technique exposes the bare substrate by removing the majority of the coating.

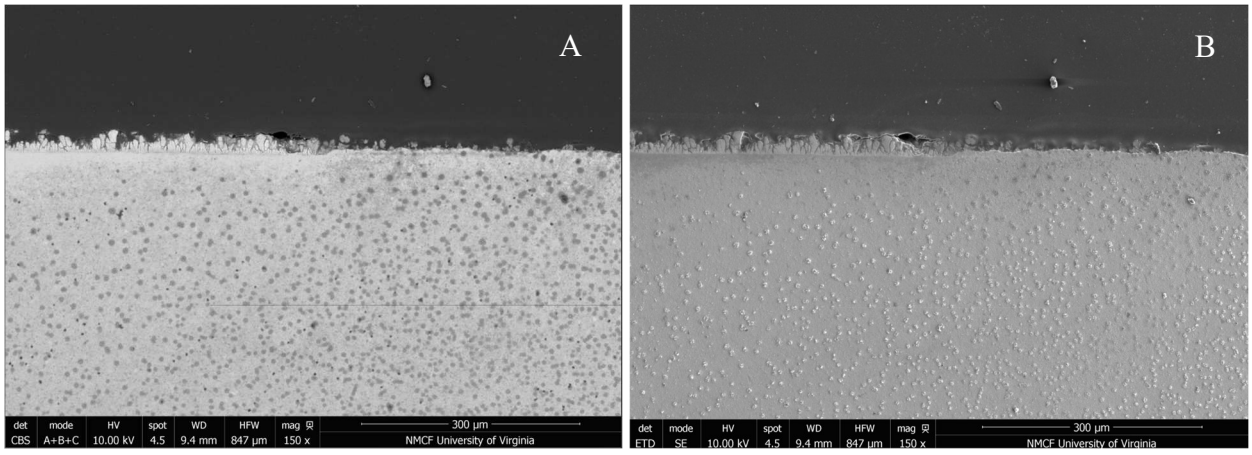

Fig. 27. Sample B3-R28 SEM micrographs that highlight the difference between the exposed and unexposed regions of the sample to the electrochemical selective dissolution in A) BSE and B) SE.

Post-Characterization: Batch 4 Sample That Reached the Immunity Potential Region

To establish the success of the selective dissolution technique, a sample from batch 4, B4-R2, underwent electrochemical treatment with a -0.5 V vs SCE limit with stirring. This process was recorded in Fig. 9. Similar to previous successful samples, much of the coating of B4-R2 was removed during treatment, seen in Fig. 28.

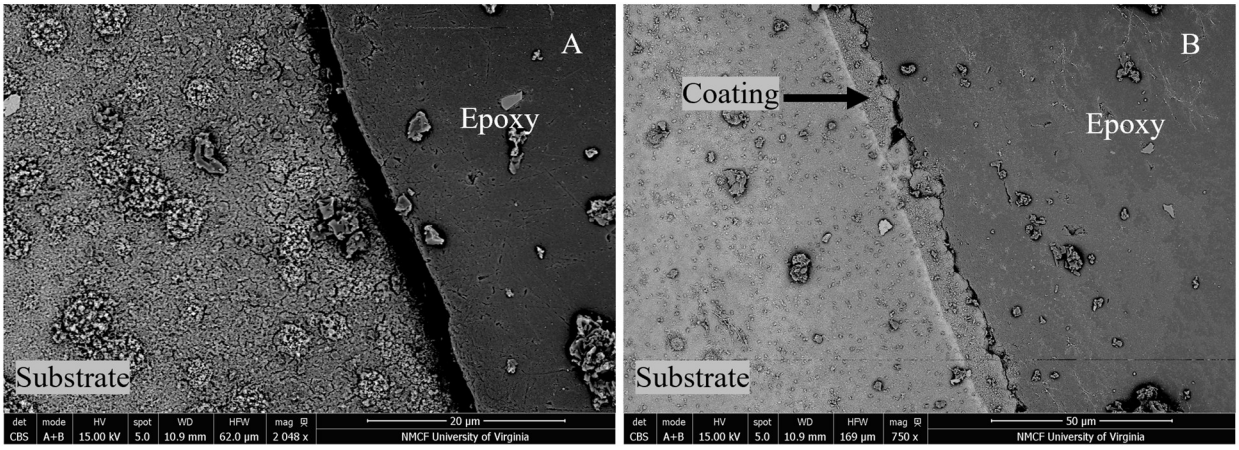

Fig. 28. BSE micrographs of B4-R2 in cross-section. A) 2000x within center of corrosion circle. B) 750x on area that was not exposed.

B4-R2 had vast stretches where the coating could not be found on its surface in areas that corresponded with the corrosion circle. This sample also had a much thinner and more uniform coating than seen in other samples, with thickness around 7um.

Discussion

Electrochemistry

Current Range and 30 Minute Time Limit

In Fig. 4, the blue line shows the magnitude of the OCP change produced by exposing a sample to 1 mA/cm2, which could positively affect the nobility, but the limited frame meant it was not the most favorable for this application. As discussed previously, Kontopanos proved the current density to eventually reach the potential region of immunity, but the time necessary was far outside of the time constraint set and supports the conclusion that this current density would not be viable for this optimized process. The upper range explored was 100 mA/cm^2, as seen in Fig. 4, dark yellow line, and the change in potential was the greatest after 30 minutes when compared to the lower current densities tested. However, this change was not continued once the sample was exposed again to the same current density for an additional 30 minute period, in fact, the high current density reduced the nobility of the sample after a second exposure. This was due to current density being too high, and dissolving Zn and Ni at similar rates, which will not lead to the potential of the sample increasing to reach the immunity potential range. The current density found to be the most viable for the selective dissolution technique was 10 mA/cm^2. This current density has the capability to achieve the dissolution necessary within the time constraint of an hour, and it remains within the potential region of mostly Zn dissolution and raises the potential of the sample into the immunity potential region.

Potential Limit and Stirring

The experimentation for sample B3-R23, as seen in Fig. 6C, the stirring period in the second OCP test proved critical for the sample reaching the immunity region. The impact of

stirring on the potential was not temporary, because the sample had a permanent increase in nobility after the stirring had ceased, as seen in Fig. 6D. Furthermore, the test for B3-R23 allowed for the implementation of a potential limit, which was -0.5 V vs. SCE. This potential indicated a drastic increase in the rate of potential change during the galvanostatic portion of the experiment that proved to be unfavorable, as seen in Fig. 5C with the higher current densities. The implementation of the potential limit and stirring in 0.6 M NaCl was critical for reliably reaching the immunity potential region for the remaining experimentation on the batch 3 samples and on a batch 4 sample. However, this potential limit may have led to excessive dissolution of the coating off the plate, which was characterized by the SEM results discussed below. For this reason, a lower potential limit was set at -0.7 V vs. SCE, as seen in Fig. 10B for sample B3-R28. This operating condition shared the same capability to raise the potential of the sample to the immunity potential region, but there were still concerns about excessive coating removal. Moreover, the OCP test that took place after the 10 mA/cm^2 galvanostatic test, did not have a stable potential reading before the stirring was engaged, as seen in Fig. 10C. Therefore, it is not possible to comment on the impact of stirring on a sample whose galvanostatic test ceased at a lower potential limit.

Repeatability of Reaching Potential Range

The selective dissolution technique for reaching the immunity potential region was a 0.01 A/cm^2 galvanostatic hold in the DIPSOL IZ-C17+ solution, before switching the solution to 0.6 M NaCl and stirring within the solution at 900 rpm for 20 minutes. The experimental parameters were repeated on sample B3-R8, as seen in Fig. 8B, to see if the results were reproducible. The repeated procedure was able to yield a stable OCP within the immunity potential region, but this occurred prior to the stirring procedure being initiated. That behavior was not seen with the previous batch 3 samples that had undergone the exact same selective dissolution technique. The varying OCP behavior was not represented with previous results, but it was still within the immunity potential region, so that cemented the current density of choice to be 0.01 A/cm^2.

Batch 4

With a repeatable technique established, it was necessary to see if it was viable on a different panel, nominally the batch 4 samples. Sample B4-R2 was tested with the procedure and parameters that had been successful with samples B3-R20, B3-R23, and B3-R8. The starting OCP of sample B4-R2 was much higher than the measured OCP with the batch 3 samples. Specifically, the OCP stabilized around -825 mV vs. SCE, which is about 150 mV higher than the batch 3 samples, seen in Fig. 4A. The behavior throughout the galvanostatic hold did not deviate from what was expected. The sample was within the immunity potential region, but it is of note that stirring did not have as drastic an effect, which can be seen in Fig. 9C. This is in comparison to batch 3 samples that underwent the same technique with the same current density. Also, once the experimentation had ceased, the sample was extremely shiny and metallic in its appearance where the dissolution process had occurred. The batch 3 samples had minimal metallic sheen, but it was extremely apparent with the batch 4 sample. The coating was removed from the sample, which is not the desired result.

XRD and SEM

Pre-Characterization of Batch 3 and Batch 4 Samples

In an effort to better understand the original plating processing and the structure that formed from it, XRD was performed. From this, there is evidence of peak broadening across all diffraction patterns. Peak broadening is an artifact of crystallite size. A broader peak indicates a smaller crystal size. Single crystals have strong, thin peaks that have an infinite slope because the size of the crystal is infinitely large in the frame of reference of the X-ray diffraction detector. Peak broadening is a deviation from the ideal conditions that reference cards may include, so this consideration is being made alongside XRD analysis.

The XRD data collected are typical of electrodeposited nucleation and growth patterns because there is a strong preference for one orientation, represented by the relative intensity of one peak being far greater than that of the other peaks. Due to the strong preference for one orientation, these samples cannot be described as having random grain orientations, which is the intended, ideal condition with powder XRD (p-XRD). Thus, the p-XRD reference data will have peaks that are not detected in the observed diffraction patterns. To achieve even greater confidence in the structural information garnered from XRD analysis, Dr. Diane Dickie, UVA NMCF X-Ray scientist, recommends either performing grazing incidence using the Empyrean diffractometer or performing in-plane diffraction using the SmartLab X-Ray Diffractometer produced by Rigaku.

There is evidence of consistent peak shift within each diffraction pattern. Peak shift could be related to strain, contamination, or planar misalignment in the X-ray diffractometer. These data are likely not due to planar misalignment because of the strong intensity of the preferential phase peak. Nor is contamination likely the cause, similarly because of the strength of the data, consistency among the peaks with the reference card patterns, and no artifact of amorphous materials, further disproving this possibility. Thus, it is likely the presence of strain because the peak shift is consistent across all peaks relative to the reference card and the shifts are not large.

This data proves the coating thickness to be sufficiently large for the X-rays to not detect the substrate material. It is evident that the steel substrate is not being characterized because steel is primarily comprised of iron. Iron would fluoresce with the copper source that was used and would cause the diffraction pattern to look vastly different. The fluorescence of iron would result in an uncommonly high intensity for the background. This is not displayed here, thus there is assurance that the coating is sufficiently thick, and the diffraction data is not a detection of the steel substrate.

To establish sample morphology and thickness, several samples were characterized that had not been subjected to electrochemical testing. Samples B3-R2 and B3-R3 were both analyzed by SEM as displayed in Figures ~~X-Z~~13-15. Fig. 13~~X~~ shows SE and BSE micrographs of the Zn-Ni coating in cross section on sample B3-R2. These micrographs show the variation in coating thickness on the substrate. Awareness of this variation is important, especially when considering methods to improve the selective dissolution technique. Fig. 14~~Y~~ presents the Zn-Ni surface morphology in plan view of sample B3-R3. This topography is composed of linear

nodes, seen in both SE and BSE micrographs. These nodes are consistently found on the surface of other samples, such as sample B3-R11, and are the morphological byproduct of coating deposition. Fig. 15~~Z~~ provides high magnification (5000x) micrographs of a crack propagated though one of the characteristic coating nodes in sample B3-R3. This crack could be a result of residual stresses or mechanical damage due to rough sample handling. While electrochemical testing had not been conducted on these samples, it is important to mention that the coatings of samples that did undergo selective dissolution experienced increased cracking in and between nodes and, in several spots, apparent stripping of the nodes entirely.

Samples from a second plate which underwent different plating conditions were characterized to find the compositional and morphological differences between the coatings and verify that the selective dissolution technique can be replicated across different panels. The samples B4-R3 and B4-R12 from batch 4 did not display the same linear nodes seen in batch 3. Fig 16B shows the coating as a BSE micrograph in plan view where the nodes appear more random and uniform. This is supported in cross-sectional view in Fig 16A where the coating thickness is significantly less variable. This difference in morphology may be due to a texture in the steel plate leading to preferential coating deposition along lines in batch 3 compared to batch 4 having a more uniform deposition. In electrodeposition, the thickness of the coating can vary across the same plate. Sample B4-R3 had a similar thickness distribution compared to batch 3 samples, but only barely reached 20µm at the thickest points. This indicates that batch 4 has a thinner coating than batch 3. The samples were not labeled with their original position prior to sectioning, so the tested samples could have come from different portions of the plates, contributing to this difference in thickness.

Surface Impact and Coating Thickness of Samples after 30 Minute Tests

Electron microscopy performed on cross-section samples B3-R5 and B3-R9 show that the thickness of the coating is not significantly altered by dissolution experiment. However, the appearance of B3-R5, B3-R20, and B3-R23 differ greatly. The potential recorded for those samples suggest that the plating has been diminished to reveal the more noble substrate.

On the surface of sample B3-R11, there are breaks in the lines of nodes shown uniformly within the selective dissolution exposed area that were not seen prior to exposure or in regions not exposed. This could be cracking due to the stress from dissolution, or it could be preferential Zn dissolution. Seen in Fig. 22, this separation does not correspond with current density as sample B3-R11 (0.1 A/cm^2) displays less significant separation than B3-R23 (0.01 A/cm^2), which reached the immunity potential region. The main difference in the experimental process with these samples was that sample B3-R23 experienced the passivation potential jump during the galvanostatic hold, leading to an increase of passivating corrosion product on the surface. Whereas the galvanostatic hold for sample B3-R20 ceased at -0.5 V vs. SCE, limiting the amount of corrosion product on its surface.

In BSE micrographs, commonly referred to as compositional SEM, elements with higher atomic numbers (Z) appear lighter due to an increase in atomic scattering efficiency. The lighter regions are Zn rich compared to the darker regions Zn has a higher Z than Ni. The compositional micrograph of B3-R11 in Fig. 22 A) reveals that the selective dissolution process has been

successful in preferentially removing Zn as the exposed region is much darker than the unexposed region. The affected region displayed non-uniform dealloying along the edges, seen in all samples.

Surface Impact and Coating Thickness of Samples That Reached Potential Immunity Range

For the samples that reached the immunity potential region, the coating was severely changed with large portions of it stripped from the surface of the substrate. Samples B3-R20 and B3-R23 are shown in plan view and only sparse amounts of the Zn-Ni coating remains could be seen. Not all of the coating was stripped, but it appears to be more drastic the closer towards the center of the selective dissolution exposed area it is. Near the edge of the exposed area, near the gasket contact, corrosion products and far more coating remnants were present compared to the center of the exposed area, as seen in Fig. 24. This is further supported by cross-sectional micrographs, where large portions of the coating could not be found. Due to particulate obfuscation and time constraints, the exact percentage of how much coating was removed is unclear.

It was deduced that the success of the selective Zn depletion could be thickness dependent. This conclusion was produced by macroscopic observation after experimentation, noting that post-experimentation, sample B4-R2 had a shinier finish, indicating that more of the coating had been stripped away to reveal the substrate beneath. This sample from batch 4, had a coating that was significantly thinner than that of batch 3. The coating thickness for batch 4 averaged around 7µm compared to the thickness ranges seen in batch 3 with an upper bound of around 25 to 30um. However, sample B4-R2 also displayed a much more uniform distribution of thickness than observed in other samples.

EDS scans were taken on the successful selective dissolution cross-sectioned samples, but the data did not seem appreciable, as most of the coating in regions of interest were stripped away to reveal to steel substrate. Sample B3-R20 shows that the coating was completely removed in the exposed region. EDS scans in Fig. 25 reflected the absence of Zn-Ni. This is further evidenced below with Sample B3-R28 in Fig. 29~~Ɣ~~. and 30~~Ƶ~~.

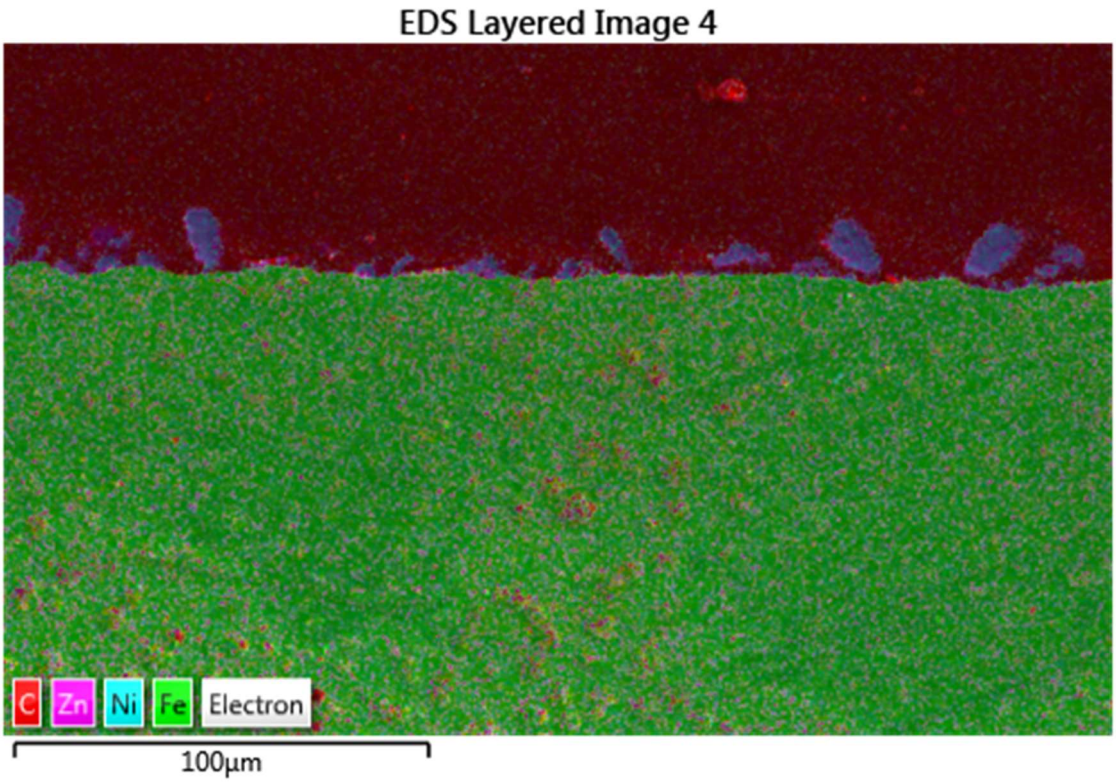

Fig. 29. Sample B3-R28 was taken to EDS after selective dissolution and there was not a continuous Zn-Ni coating left on the surface. This is shown in this compositional map.

A B

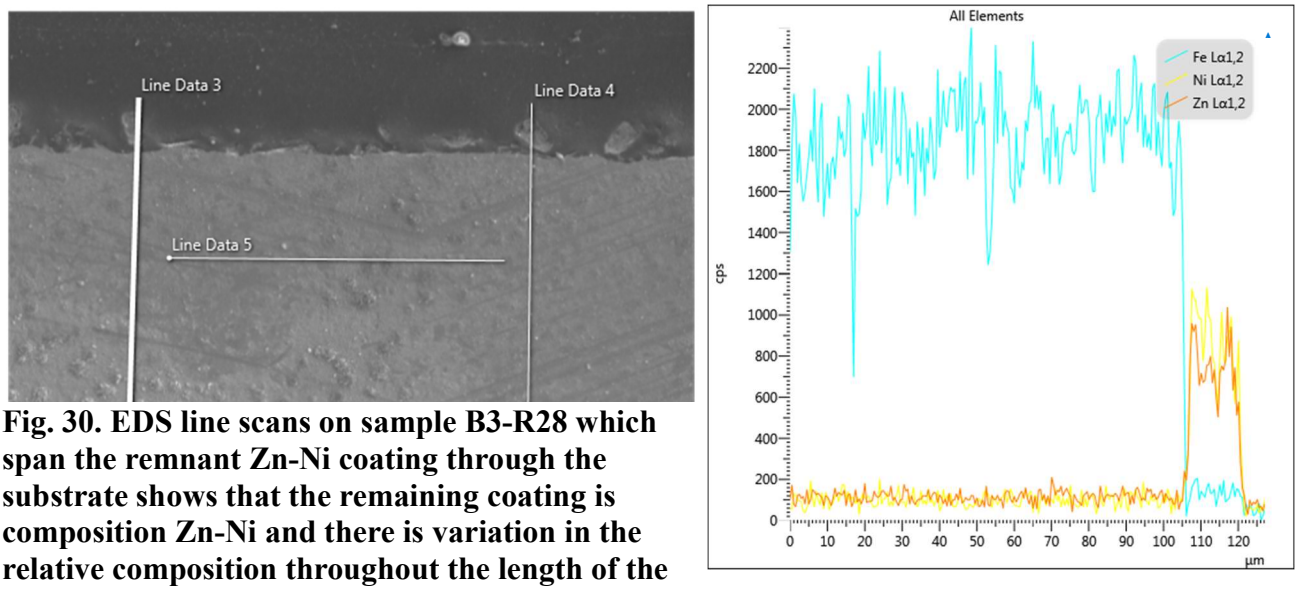

Fig. 30. EDS line scans on sample B3-R28 which span the remnant Zn-Ni coating through the substrate shows that the remaining coating is composition Zn-Ni and there is variation in the relative composition throughout the length of the remnant Zn-Ni.

The line scan begins at the coating and ends at the point on the end of the line in the bulk. There is a background signal in Fig. 30 B) of Zn-Ni being present in the steel, which is not representative of the true composition. This background should be subtracted from the conclusions drawn from this data, because it is apparent that there is Zn-Ni in the coating and Fe in the bulk.

The recorded final OCP was more noble than the initial OCP, indicating that either the Zn depleted coating is more abundant than it appears or that the coating was stripped so severely that the more noble potential of the substrate is influential. Based on the appearance of the coating after the selective dissolution technique in plane and cross-sectional view, the latter option seems more likely.

Conclusions and Future Work

Conclusions

The team has designed and executed several prototypes of a selective dissolution technique to reach a measured final OCP value within the target region to mitigate SCC. These experiments have been informed by simultaneous electron microscopy. Through characterization, it was identified that the surface morphology and corrosion products changed the electrochemical plating processing through SEM which coincided with the electrochemical data produced. Executed treatment varied procedure, current density, and length of conditions until the potential region of interest was achieved. When this potential region of interest was achieved, post-experimental SEM showed the coating was completely removed. Furthermore, EDS results indicated that there was no presence of Zn or Ni on the surface steel substrate. This was investigated using specimens from both batch 3 and batch 4. The samples from batch 4 appeared to consistently have thinner Zn-Ni coatings on average. In both cases, the coating was stripped down to the substrate. Thus, the change in OCP to the region of interest was most likely not due to the selective dissolution of Zn from the Zn-Ni coating, but due to the exposure of the more noble substrate material.

Future Work

Potential Limit Optimization

A lower potential limit was able to deplete less of the substrate coating compared to a higher potential limit during the galvanostatic portion of the selective dissolution technique. Also, the lowered potential limit was able to reach the immunity potential region of interest. Further work could be done to ascertain the potential limit that would allow the selective dissolution process to dissolve enough Zn to reach the immunity potential region, while also maintaining the structural integrity of electrodeposited coating.

Samples with Carbon Steel as the Substrate

The samples that were tested throughout this project were comprised of a carbon steel substrate. This substrate is different than the in-use substrate that will be implemented by RR, which is a Pyrowear steel alloy. Pyrowear is an expensive specialty alloy and thus, it is not economically feasible to perform research and development with this substrate and a cheaper carbon steel is used in its place. The electrochemical properties of these differing substrates vary under the testing conditions done. This contrast in properties is exacerbated due to this technique revealing the underlying substrate. Extending the technique testing to include coated Pyrowear substrates would highlight the impact on OCP that was a product of the exposed carbon steel due to excessive dissolution, as opposed to a representative result across steels.

Capability of this Technique on Thicker Coatings

The thickness of each coating can be determined through cross-sectional microscopy and analysis. With electroplating, thickness can be variable across a single plate and thus, must be a consideration during processing. The technique and its utility could be further understood if through a wider sample test matrix including samples with a thicker coating. This would then

prevent risk of substrate exposure, which occurred during this project. Thus, this sample condition expansion would prove critical for evaluating if the technique would be capable of reaching the immunity potential region through Zn dissolution alone; as opposed to, only reaching the immunity potential region to the underlying substrate being exposed because to the plated coating is too thin.

Acknowledgements

We would like to thank Dr. James Fitz-Gerald for advising in the capstone project and Dr. Robert Kelly and Victor Kontopanos for lending their lab space and expertise. We would also like to thank Dr. Robert Golden and Brad Wiley of Rolls-Royce and Dr. Rebecca Marshall and Victoria Avance of Luna Labs USA for providing industry representation and guidance for the project.

References

Harris, Z. D., Marshall, R. S., Kelly, R. G., and Burns, J. T. (2023). Coupling Fracture Mechanics Experiments and Electrochemical Modeling to Mitigate Environment-Assisted Cracking in Engineering Components. *Corrosion, 79*(3), 363-375. https://doi.org/10.5006/4244.